Journal of Hazardous Materials 211–212 (2012) 317–331

Contents lists available at SciVerse ScienceDirect

Journal of Hazardous Materials

journal homepage: www.elsevier.com/locate/jhazmat

Review

Heavy metal removal from water/wastewater by nanosized metal oxides: A review

Ming Hua, Shujuan Zhang, Bingcai Pan*, Weiming Zhang, Lu Lv, Quanxing Zhang

State Key Laboratory of Pollution Control and Resource Reuse, School of the Environment, Nanjing University, Nanjing 210046, PR China

ARTICLE INFO

Article history:
Received 8 June 2011
Received in revised form
29 September 2011
Accepted 4 October 2011
Available online 8 October 2011

Keywords:
Nanosized metal oxides
Heavy metals
Removal
Water treatment
Hybrid adsorbent
Nanocomposite

ABSTRACT

Nanosized metal oxides (NMOs), including nanosized ferric oxides, manganese oxides, aluminum oxides, titanium oxides, magnesium oxides and cerium oxides, provide high surface area and specific affinity for heavy metal adsorption from aqueous systems. To date, it has become a hot topic to develop new technologies to synthesize NMOs, to evaluate their removal of heavy metals under varying experimental conditions, to reveal the underlying mechanism responsible for metal removal based on modern analytical techniques (XAS, ATR-FT-IR, NMR, etc.) or mathematical models, and to develop metal oxide-based materials of better applicability for practical use (such as granular oxides or composite materials). The present review mainly focuses on NMOs' preparation, their physicochemical properties, adsorption characteristics and mechanism, as well as their application in heavy metal removal. In addition, porous host supported NMOs are particularly concerned because of their great advantages for practical application as compared to the original NMOs. Also, some magnetic NMOs were included due to their unique separation performance.

Contents

Abbreviations: NMOs, nanosized metal oxides; NFeOs, nanosized Fe oxides; NMnOs, nanosized Mn oxides; HFO, hydrous Fe oxides; HMO, hydrous Mn oxides; HAO, hydrous Al oxides; OMS, octahedral molecular sieve; TEM, transmission electron microscopy; BET, Brunauer–Emmett–Teller (triple-point N_2 Brunauer–Emmett–Teller adsorption isotherm); XRD, X-ray diffraction; XPS, X-ray photoelectron spectroscopy; VSM, vibrating sample magnetometer; pH_{pzc}, pH of zero point of charge.

* Corresponding author. Tel.: +86 25 8968 0390.
E-mail address: bcpan@nju.edu.cn (B. Pan).

0304-3894/$ – see front matter © 2011 Elsevier B.V. All rights reserved.
doi:10.1016/j.jhazmat.2011.10.016

1. Introduction

Exposure to heavy metals, even at trace level, is believed to be a risk for human beings [1–4]. Thus, how to effectively and deeply remove undesirable metals from water systems is still a very important but still challenging task for environmental engineers. Nowadays, numerous methods have been proposed for efficient heavy metal removal from waters, including but not limited to chemical precipitation, ion exchange, adsorption, membrane filtration and electrochemical technologies [5–9]. Among these techniques, adsorption offers flexibility in design and operation and, in many cases it will generate high-quality treated effluent. In addition, owing to the reversible nature of most adsorption processes, the adsorbents can be regenerated by suitable desorption processes for multiple use [10], and many desorption processes are of low maintenance cost, high efficiency, and ease of operation [11]. Therefore, the adsorption process has come to the forefront as one of the major techniques for heavy metal removal from water/wastewater.

Among the available adsorbents, nanosized metal oxides (NMOs), including nanosized ferric oxides, manganese oxides, aluminum oxides, titanium oxides, magnesium oxides and cerium oxides, are classified as the promising ones for heavy metals removal from aqueous systems [12–14]. This is partly because of their large surface areas and high activities caused by the size-quantization effect [15,16]. Recent studies suggested that many NMOs exhibit very favorable sorption to heavy metals in terms of high capacity and selectivity, which would result in deep removal of toxic metals to meet increasingly strict regulations [17]. However, as the size of metal oxides reduces from micrometer to nanometer levels, the increased surface energy inevitably leads to their poor stability. Consequently, NMOs are prone to agglomeration due to Van der Waals forces or other interactions [18], and the high capacity and selectivity of NMOs would be greatly decreased or even lost. Moreover, NMOs are unusable in fixed beds or any other flow-through systems because of the excessive pressure drops (or the difficult separation from aqueous systems) and poor mechanical strength. To improve the applicability of NMOs in real wastewater treatment, they were then impregnated into porous supports of large size to obtain composite adsorbents [10]. The widely used porous supports include activated carbon, natural materials, synthetic polymeric hosts, etc.

Besides traditional NMOs, magnetic NMOs attract increasing attentions because they can be easily separated from water under a magnetic field [19]. Also, magnetic NMOs-based composite adsorbents allowed easy isolation from aqueous solutions for recycling or regeneration [20]. Such facile separation is essential to improve the operation efficiency and reduce the cost during water/wastewater treatment.

This review presented a brief view on several typical NMOs, including their synthesis and characterization, their sorption behavior of heavy metals (e.g., Pb (II), Cd (II), Cr (VI), and Cu (II)) from aqueous systems under varying experimental conditions, the underlying mechanism responsible for the sorption, as well as their reusability. Porous host supported NMOs were briefly introduced according to the type of host materials, such as natural clay, membrane, and polymers. In addition, magnetic NMOs were summarized for their preparation and adsorptive performance on heavy metals.

2. Nanosized metal oxides

For adsorption of heavy metals from aqueous systems, the most widely studied NMOs include iron oxides, manganese oxides, aluminum oxides, and titanium oxides. They are present in different forms, such as particles, tubes and others (Table 1). The size and shape of NMOs are both important factors to affect their adsorption performance. Efficient synthetic methods to obtain shape-controlled, highly stable, and monodisperse metal oxide nanomaterials have been widely studied during the last decade. Generally, the synthesis methods can be classified into two categories: (1) physical approaches, including inert gas condensation, severe plastic deformation, high-energy ball milling, ultrasound shot peening, and (2) chemical approaches, including reverse micelle (or microemulsion), controlled chemical co-precipitation, chemical vapor condensation, pulse electrode position, liquid flame spray, liquid-phase reduction, gas-phase reduction, etc. [38]. Among these synthesis protocols, co-precipitation [39,40], thermal decomposition and/or reduction [41], and hydrothermal synthesis [42] techniques are used widely and are easily scalable with high yields [43]. As for the characterization of NMOs, research efforts focused on their characteristics, such as morphology, size, crystal structure, specific surface area and the pH of zero point of charge (pH_{pzc}). The most widely used techniques and tools for this purpose are summarized in Table 2.

In the following sections, recent advances in heavy metal removal from water and wastewater by NMOs are presented in terms of their synthesis, characterization, and application perspectives and are classified by the components of NMOs.

2.1. Nanosized ferric oxides

Iron is one of the most widespread elements in the earth. The facileness of resource and ease in synthesis render nanosized ferric oxides (NFeOs) to be low-cost adsorbents for toxic metal sorption. Since elemental iron is environmentally friendly, NFeOs can be pumped directly to contaminated sites with negligible risks of secondary contamination [51]. The intensively studied NFeOs for heavy metals removal from water/wastewater include goethite (α-FeOOH), hematite (α-Fe_2O_3) [21,22], amorphous hydrous Fe oxides [23], maghemite (γ-Fe_2O_3) [24,25], magnetite (Fe_3O_4) [19,44,52–55] and iron/iron oxide (Fe@Fe_xO_y) [50].

2.1.1. Goethite (α-FeOOH) and hematite (α-Fe_2O_3)

The chemical nature and the high specific surface area of goethite make it an efficient sorbent for metal cations [56]. Grossl et al. [21] evaluated the kinetics of Cu^{2+} adsorption/desorption on/from goethite (α-FeOOH) using the pressure-jump (p-jump) relaxation technique, which provides both kinetic and mechanistic information for reactions occurring on millisecond time scales. Adsorption of Cu (II) increased with the increasing pH from 4.5 to 5.5. The process was insensitive to the background electrolytes. Cu (II) sorption on nano-goethite surface was found to form an

Table 1
NMOs for heavy metal removal from water.

Adsorbent	Preparation	Shape and size (nm)	Surface area (m^2/g)	Target metals	Temperature	Performance	Isotherm model	Refs.
Goethite (α-FeOOH)	$Fe(NO_3)_3$ precipitation	Needlelike; length 200 nm; width <50 nm	50	Cu (II)	25 ± 0.1 °C	100% removal (pH = 6.0); intrinsic adsorption rate constant, $10^{6.81}$ L mol^{-1} s^{-1}; desorption rate constant, $10^{4.88}$ L mol^{-1} s^{-1}	–	[21]
	Coprecipitation: HCl and $FeCl_3$ solution at 100 °C for 2 days	Width, 10–15 nm; length, 500 nm	71.49	Cu (II)	25 °C	149.25 mg/g (pH = 5.2 ± 0.1)	Langmuir isotherm	[22]
Hematite (α-Fe_2O_3)	Coprecipitation: $Fe_2(SO_4)_3$ + 2.5 M NaOH (4 h), heated at 40 °C for 2 days	Granular, with a crystal size about 75 nm	24.82	Cu (II)	25 °C	84.46 mg/g (pH = 5.2 ± 0.1)	Langmuir isotherm	[22]
Hydrous amorphous Fe oxides	Participation: $Fe(NO_3)_3$ + NaOH	Particles; diameter, 3.8 nm	600	Pb (II)	25 °C	Surface diffusivities 1.4×10^{-15} cm^2 s^{-1}	–	[23]
γ-Fe_2O_3	Sol–gel method	Particles; diameter, 10 nm	178	Cr (VI)	22.5 °C	Max capacity is 19.2 mg/g at pH of 2–3	Freundlich isotherm	[24]
	Sol–gel method	Particles; diameter, 10 nm	198	Cr (VI), Cu (II), Ni (II)	25 °C	Equilibrium within 10 min; the optimal pH: 2.5 (Cr), 6.5 (Cu), and 8.5 (Ni); capacities: 17.0 (Cr), 26.8 (Cu), and 23.6 (Ni) mg/g	Langmuir isotherm	[25]
Hydrous manganese dioxide	Participation: $Mn(NO_3)_2$ + $NaMnO_4$ + NaOH	Particles; diameter, 2.1 nm	359	Pb (II)	25 °C	Surface diffusivities 1.7×10^{-16} cm^2 s^{-1}	–	[23]
	Precipitation: $MnSO_4$ + NaClO	Particles	100.5	Pb (II), Cd (II), Zn (II)	25 °C	Sorption preference $Pb^{2+} > Cd^{2+} > Zn^{2+}$	Freundlich model	[26]
α-MnO_2(OMS-2)	Precipitation method (refluxing)	5 nm sized octahedras with 2 × 2 tunnel size of 0.46 nm	–	Cu (II)	25 °C	Max capacity 1.3 mmol/g; distribution coefficient $K_d = 10^4$ mL/g	–	[27,28]
α-MnO_2(OMS-1)	Precipitation method (refluxing)	Octahedras with 3 × 3 tunnel size of 0.70 nm	–	Cu (II)	25 °C	Max capacity 0.9 mmol/g, distribution coefficient $K_d = 3 \times 10^4$ mL/g	–	[28]
TiO_2	Hydrolysis	Particles with size of 10–50 nm	208	Zn (II), Cd (II)	–	Capacity: 15.3 (Zn) and 7.9 (Cd) mg/g	–	[29]
	Commercially available	Particles, 8.3 nm	185.5	Pb (II), Cd (II), Ni (II),	25 °C	q_m = 401.14 (Pb), 135.14 (Cd), 114.94 (Ni) (μmol/g); K_d = 107–109 (Pb), 105–109 (Cd), 104–105 (Ni) (mL/g)	Langmuir isotherm	[30]
Hydrous amorphous Al oxides	Participation: NaOH + $Al(NO_3)_3$	Particles; diameter 1.9 nm	411	Pb (II)	25 °C	Surface diffusivities 6.5×10^{-16} cm^2 s^{-1}	–	[23]
γ-Al_2O_3	Precipitation	Particles with size of 7.5 nm	240	Ni (II)	20 °C	176.1 mg/g, $K_d = 5 \times 10^5 cm^3/g$	–	[31]
γ-MPTMS modified γ-Al_2O_3	Mixture	–	–	Cu (II), Hg (II), Pd (II)	–	Removal: Cu 100%, Hg 97.8–99%, Pd 97–100%	–	[32]
DNPH modified γ-Al_2O_3	Chemically immobilization	Particles, diameter 68–87 nm	42.62	Pb (II), Cd (II), Cr (III), Co (II), Ni (II), Mn (II)	–	Max capacity: 100 (Pb), 83.33 (Cd), 100 (Cr), 41.66 (Co), 18.18 (Ni), 6.289 (Mn) mg/g	Freundlich isotherm for Mn (II), Pb (II), Cr (III) and Cd (II) ions Langmuir isotherm for Ni (II) and Co (II) ions	[33]
ZnO	Hydrotherm	Nanosheets with square sides of about 1 μm and thickness in nano-scale.	–	Pb (II)	Room temperature	6.7 mg/g	–	[34]
	Solvotherm	Nanoplates of 10–15 nm in thickness and pore diameter of 5–20 nm	147	Cu (II)	25 °C	> 1600 mg/g, K_L = 0.050 L/mg	Freundlich isotherm	[35]
CeO_2	Precipitation	Hollow nanospheres, with a uniform size of 260 nm, composed of CeO_2 nanoparticles of about 14 nm.	72	Cr (VI) Pb (II)	Room temperature	15.4 mg/g (Cr), 9.2 mg/g (Pb)	Langmuir isotherm	[36]
	Precipitation	Particles with mean size 6.5–12 nm	65	Cr (VI)	Room temperature	121.95 mg/g	Freundlich isotherm	[37]

Table 2
Characterization of NMOs and NMOs-based sorbents form heavy metals removal from water/wastewater.

Characteristics	Techniques	Targeted sorbents
Morphology	Transmission electron microscopy (TEM).	Goethite [21], maghemite [24,25], amino-functionalized Fe_3O_4@SiO_2 [44], HAO, HFO, HMO, HAO-coated montmorillonite [23]
	Environmental scanning electron microscope (ESEM)	HAO, HFO, HMO, HAO-coated montmorillonite [23]
	Field emission scanning electron microscope (FE-SEM)	HAO, HFO, HMO, HAO-coated montmorillonite [23]
Particle size	Laser diffraction particle size analyzer	γ-Fe_2O_3 [45]
Crystal structure	X-ray diffraction (XRD)	Goethite [21,22], HAO, HFO, HMO, HAO-coated montmorillonite [23], amino-functionalized Fe_3O_4@SiO_2 [44], maghemite [22,24,25], Fe_3O_4 and Fe_3O_4–PEDOT [46]
Specific surface area	Triple-point N_2 Brunauer–Emmett–Teller (BET) adsorption	Goethite [21,22], HAO, HFO, HMO, HAO-coated montmorillonite [23], Maghemite [24,25], amino-functionalized Fe_3O_4@SiO_2 [44]
pH_{pzc}	Potentiometric titration	HAO, HFO, HMO, HAO-coated montmorillonite [23]
	Zeta potential analyzer	Maghemite [24]
Heavy metal-NMO interaction	Extended X-ray absorption fine structure (EXAFS) spectroscopy	Nanosized manganese oxide [47,48]
	X-ray absorption near edge structure (XANES) spectroscopy	Nanosized cerium and titanium dioxides [49]
	X-ray photoelectron spectroscopy (XPS)	Maghemite [24,25], Fe@Fe_xO_y [50], Amino-functionalized Fe_3O_4@ SiO_2 [44]
	UV–Vis diffuse reflectance spectrometer	Goethite and hematite [22]
	Diffuse-reflectance infrared Fourier transform (DRIFT) spectra	Fe_3O_4 and Fe_3O_4–PEDOT [46]
	FTIR	Amino-functionalized Fe_3O_4@ SiO_2 [44], γ-Fe_2O_3 [45]
	Raman spectroscopy	Maghemite [24,25]
	C^{15} peak	Amino-functionalized Fe_3O_4@ SiO_2 [44]
Magnetic properties	Vibrating sample magnetometer (VSM)	Maghemite [24,25], Amino-functionalized Fe_3O_4@SiO_2 [44], γ-Fe_2O_3 [45]
	External magnetic fields	Fe_3O_4 and Fe_3O_4–PEDOT [46]

inner-sphere surface complex, which was further demonstrated by the modified triple-layer model simulation with the experimental data. The calculated intrinsic rate constant for adsorption ($10^{6.81}$ L mol^{-1} s^{-1}) was about two orders of magnitude higher than the intrinsic rate constant for desorption ($10^{4.88}$ L mol^{-1} s^{-1}). The rate of adsorption of divalent metal cation on goethite is directly related to that of water molecule release from the primary hydration sphere of a specific divalent metal cation. The conjunction of p-jump technique and surface complexation modeling is also employed to describe Cu^{2+}, Pb^{2+}, Zn^{2+}, Co^{2+}, and Mn^{2+} adsorption/desorption on γ-Al_2O_3 [57] and Pb^{2+} adsorption/desorption on α-FeOOH (goethite) [58]. Analysis by Eigen and Tamm steady-state model [59] further implied that the divalent metal cations usually form inner-sphere surface complexes with the oxide surfaces.

Fig. 1 represents the TEM images of nano-goethite and nano-hematite [22]. Cu^{2+} adsorption on nano-hematite was similar to nano-goethite in terms of kinetics and dynamics, while nano-goethite showed a larger specific surface and a higher maximum Cu^{2+} adsorption capacity than those of nano-hematite (71.49 m^2/g vs 24.82 m^2/g; 149.25 mg/g vs 84.46 mg/g) [22]. The adsorption of Cu^{2+} on both NFeOs was a spontaneous process and followed the pseudo-second-order kinetics. Their adsorption isotherms were better described by the Langmuir model (R^2 = 0.96–0.98) than the Freundlich model (R^2 = 0.56–0.57), suggesting that the active sites on their surface were homogeneous for Cu^{2+} sorption [22].

2.1.2. Hydrous ferric oxide

Hydrous ferric oxide (HFO) could be prepared by precipitation of ammonia with ferric chloride or nitrate solutions in carbonate-free environment by purging with N_2 [23]. In this way, Dzombak and Morel [60] produced HFO with mean pore diameter of 3.8 nm and surface area of 600 m^2/g.

The sorption of heavy metals to HFO seems poorly sensitive to the variation of ionic strength. For example, Swallow et al. [61] reported that Cu^{2+} and Pb^{2+} sorption to HFO was unaffected by different ionic strength from 0.005 to 0.5 M $NaClO_4$, or by change in the nature of the background electrolyte from $NaClO_4$ to a complex artificial seawater mixture. Trivedi et al. [62] observed that Pb^{2+} sorption to ferrihydrite did not vary with ionic strength in the range between 10^{-3} and 10^{-1} M $NaNO_3$. The resistance to variation in ionic strength might suggest the formation of inner-sphere complexes between heavy metals and HFO. Intraparticle diffusion, a natural attenuating process, was observed to be the rate-limiting step in the sorption process of Pb^{2+} on HFO nanoparticles. The process could be described by two steps: a rapid adsorption of metal ions to the external surface followed by a slow intraparticle diffusion along the micropore walls [23].

2.1.3. Maghemite (γ-Fe_2O_3) and magnetite (Fe_3O_4)

Maghemite (γ-Fe_2O_3) nanogels can be prepared by a sol–gel method, that is, adding NH_4OH solution to the mixture of $FeCl_3$ and $FeCl_2$ in the purified water deoxygenated and bubbled by nitrogen gas. The product was red-brown γ-Fe_2O_3 nanogel and was collected via external magnetic field after adding ethanol. The prepared maghemite nanoparticles are expected to respond well to magnetic fields without any permanent magnetization, because the saturation moment of the synthesized particles, as determined by the hysteresis loop measured from vibrating sample magnetometer (VSM), was similar to the value of the bulky particles (3.3 emu/g vs 3.4 emu/g) [24]. The TEM images revealed that the maghemite nanoparticles synthesized in sol–gel method were multidispersed with an average diameter of around 10 nm. The BET surface area of the freeze-dried material was 178–198 m^2/g [24,25].

Hu et al. [24] examined Cr (VI) removal by nano-maghemite and found that the equilibrium period was independent of initial Cr (VI) concentration and the adsorptive capacity increased when pH decreased. Nano-maghemite emerged a high selectivity for Cr (VI) from water. Negligible competition was observed for many coexisting ions. The adsorption capacity of nano-maghemite for Cr (VI) (19.2 mg/g) is higher than that of diatomite (11.55 mg/g) [63], anatase (14.56 mg/g) [64], commercial activated carbon (15.47 mg/g) [65], and beech sawdust (16.13 mg/g) [66]. Based on X-ray diffraction (XRD), X-ray photoelectron spectroscopy (XPS), and Raman spectroscopic techniques, it could be deduced that no chemical redox reaction occurred during Cr (VI) retention, which also hints the stability of nanoscale γ-Fe_2O_3. The adsorption mechanism of Cr (VI) onto γ-Fe_2O_3 is suggested to be electrostatic attraction particularly at a relatively low pH.

A further study was carried out to investigate the adsorption kinetics and mechanisms of multiple heavy metals [25], Cr (VI), Cu

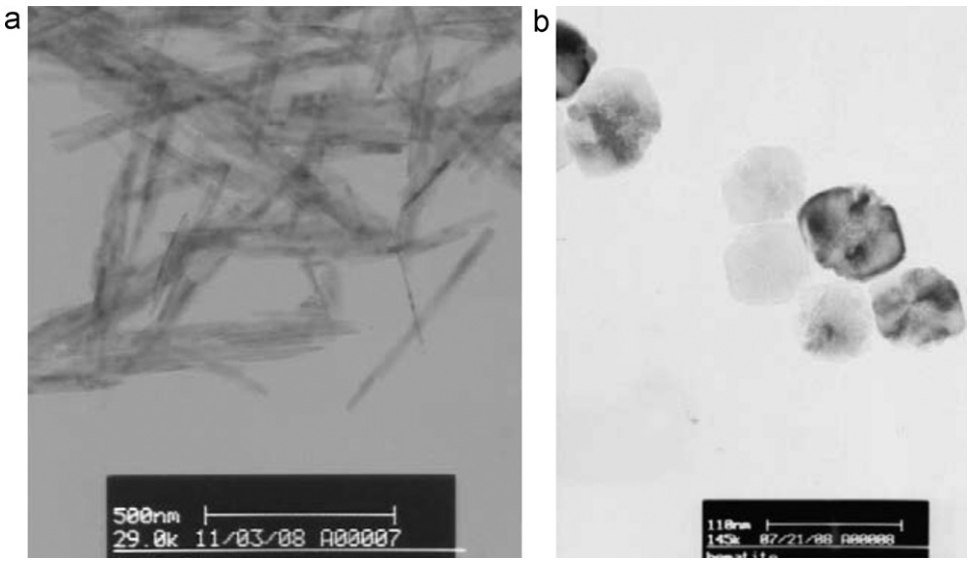

Fig. 1. TEM images of (a) nano-goethite and (b) nano-hematite [22].

(II), and Ni (II), by maghemite nanoparticles. All the adsorption was highly pH dependent. The optimal pH for the selective removal of Cr (VI), Cu (II), and Ni (II) were 2.5, 6.5, and 8.5, respectively. Under the optimal pH, their uptakes mainly resulted from electrostatic attraction.

Another important magnetic nanomaterial is nanosized magnetite. Chemical co-precipitation has been widely used to prepare magnetite nanoparticles by adding alkaline carbonate into solution containing Fe^{2+} and Fe^{3+} in a molar ratio of 1:2 [67,68]. It was found that the particle size was reduced when a surfactant (such as oleic acid) was used during the preparation [69]. Two methods were reported to prevent the change of the ratio caused by air oxidation. One is to conduct the reaction under an inert environment with nitrogen gas. Another is to set the initial Fe^{3+}:Fe^{2+}molar ratio less than 2:1 so that after the oxidation of Fe^{2+} to Fe^{3+}, the ratio approaches to 2:1 [70–73]. In addition, nano-Fe_3O_4 will be oxidized to nano-γ-Fe_2O_3. The size of the resultant Fe_3O_4 or γ-Fe_2O_3 hydrosols were considerably smaller than that reported in the literature [53,74–76] and no surfactants are needed to stabilize the sols. A decrease of specific saturation magnetization (σ_s) value was observed when the nanoparticles were coated with oleic acid. Scanning electron micrograph showed that the prepared Fe_3O_4 nanoparticle sol had an average diameter of 8.5 ± 1.3 nm, where needlelike γ-Fe_2O_3 nanoparticles with lengths of 20–50 nm and widths of 4–6 nm are visible [77]. For removal of heavy metals, nano Fe_3O_4 was commonly used as the magnetic core for composite sorbents [19,44,46,53,54,75,78].

2.2. Nanosized manganese oxides

Nanosized manganese oxides (NMnOs) exhibit an adsorptive performance superior to its bulk counterpart because of its polymorphic structures and higher specific surface area [79]. In the past decades, NMnOs have been exploited [80,81] for sorption of cationic or anionic pollutants from natural waters, such as heavy metal ions [82], arsenate [83], and phosphate [84]. Such sorption processes significantly mediate the fate and mobility of the targeted pollutants in water [26,85,86]. The widely studied NMnOs for environmental concerns include hydrous manganese oxide (HMO) and nanoporous/nanotunnel manganese oxides.

2.2.1. Hydrous manganese oxide

As reported by Parida et al. [87], HMO could be prepared by adding $MnSO_4 \cdot H_2O$ into NaClO solution (containing active chlorine). The precipitate was washed with HCl to remove excessive alkali, followed by rinsing with double-deionized water. The BET surface area is around 100.5 m^2/g. Gadde and Laitinen [88] proposed another approach for HMO synthesis, i.e., adding manganese nitrate into alkaline sodium permanganate solution and re-dispersing the particles in sodium nitrate solution. The BET surface of the resultant HMOs is 359 m^2/g.

Heavy metal sorption onto HMOs, including Pb (II), Cd (II), and Zn (II), usually results in the inner-sphere complex formation, and it can be described by an ion-exchange process. Divalent metals on HMO consist of two similar steps as that of HFO: rapid adsorption of metal ions to the external surface followed by a slow intraparticle diffusion along the micropore walls [23]. The adsorption can be represented by the Freundlich model more reasonably than the Langmuir model, implying that the active sites of HMO surface are heterogeneous for metal sorption. HMO prefers metal sorption in the order of $Pb^{2+} > Cd^{2+} > Zn^{2+}$, which might rest on the different softness of these metals [89]. Compared to two commercial resins, D-001 and Amberlite IRC 748, HMO exhibits more selective sorption toward these heavy metal ions in the presence of Ca^{2+} at high concentration levels [26].

2.2.2. Mixed-valence manganese oxides

Mixed-valence manganese oxides with 3–6 layers and 7–11 tunnel structures are classified as potentially interesting sorbents for cations. They are usually present as octahedral molecular sieve (OMS). Cryptomelane-type (K^+) and todorokite-type (Mg^{2+} and Ca^{2+}) manganese oxides, called OMS-2 and OMS-1, respectively, could be prepared by means of hydrothermal route [28,90,91]. The structures of the products are shown in Fig. 2. They have OMS structure constructed from edge sharing double chains of MnO_6 octahedra that build a 2×2 or 3×3 tunnel structure. The dimension of tunnels of OMS-1 and OMS-2 vary slightly depending on the type of the inside located cations. This feature enables small adjustments of the tunnel size and makes the material as adjustable molecular sieve. The size of the tunnels in 3×3 OMS-1(Mg^{2+}) and in 2×2 OMS-2(K^+) is about 0.7 and 0.46 nm.

Dyer et al. [92] studied the sorption behavior of radio nuclides on crystalline synthetic tunnel manganese oxides. Trace strontium (^{89}Sr) and cesium (^{137}Cs) ions were removed through ion-exchange

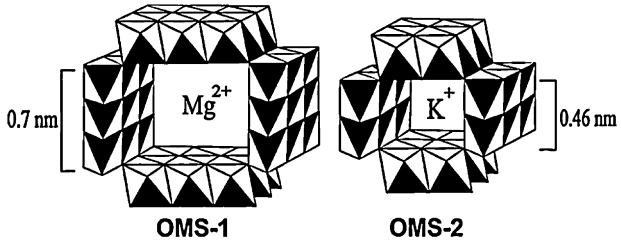

Fig. 2. Tunnel structure with the template ions of OMS materials [28].

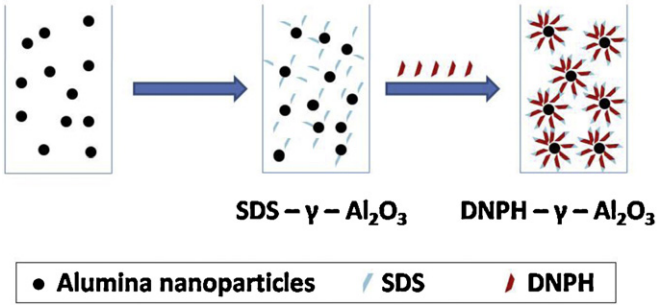

Fig. 3. Schematic illustration of functionalizing DNPH on alumina nanoparticles [33].

mechanism. Selectivity coefficients were estimated as $K_{Cs/K} = 0.6$ and $K_{Sr/K} = 1.0$ for OMS-2 and $K_{Cs/Mg} = 7550$, $K_{Sr/Mg} = 50$, and $K_{Sr/Ca} = 10$ for OMS-1. Also, it was observed that OMS-2 was particularly effective for the separation of trace silver ions. The affinity sequence for magnesium and calcium ion-extracted OMS-1 in HNO_3 was $^{137}Cs > {}^{59}Fe > {}^{51}Cr \approx {}^{57}Co \approx {}^{241}Am > {}^{54}Mn > {}^{63}Ni > {}^{65}Zn > {}^{236}Pu > {}^{89}Sr$. As examined by Pakarinen et al. [28], OMS materials exhibited selective adsorption of Cu^{2+}, Ni^{2+} and Cd^{2+} in the presence of Ca^{2+} and Mg^{2+}. The exchange rates were reasonably high due to the small particle dimensions. OMS materials are stable and their maximum Cu^{2+} uptake capacity was 0.9–1.3 mmol/g.

Koivula et al. [27] found that hydrometallurgical wastewater (containing Al, Ca, Fe, Mg, Mn and Na) rich in manganese can be easily used as a manganese precursor for OMS synthesis. A synthetic raffinate solution, which contained 4500, 490, 300, 150, 200 and 3500 mg/L of Mn, Mg, Fe, Al, Ca and Na, respectively, could be used as the manganese source for preparing OMS-2. The adsorptive selectivity (Co > Cd > Ni) is in line with the findings reported by Tsuji and Komarneni [93] and Dyer et al. [92].

In fact, manganese oxides with tunnel structures constitute a large class of selective ion exchangers and sorbents [92]. In addition to the synthetic cryptomelane- (2×2) and todorokite-type (3×3) materials, there are several other structure types such as romanechite (2×3) and RUB-7 (2×4). The selectivity of these exchangers toward metal ions greatly depends on their structures.

2.3. Nanosized aluminum oxides

Alumina (Al_2O_3) is a traditional adsorbent for heavy metals, and γ-Al_2O_3 is anticipated to be more adsorptive active than α-Al_2O_3 [94,95]. Nanosized γ-Al_2O_3 [96] can be prepared by sol–gel method and has been employed as solid phase extraction material for separation/preconcentration of trace metal ions.

Chemical or physical modification of γ-Al_2O_3 nanoparticles with certain functional groups containing some donor atoms such as oxygen, nitrogen, sulfur and phosphorus is expected to improve their sorption toward heavy metals [97–100]. When a modifier is immobilized at the surface of alumina, the removal mechanism is changed accordingly. The target metals are not only removed by adsorption on the surface of the alumina but also by a surface attraction/chemical-bonding interaction on the newly added chemicals. A very common procedure to deposit an organic coating on inorganic oxide is to mix the organic solution with inorganic oxide particles for a period of time, followed by evaporation of the solvent and air-drying the resultant adsorbent [32]. For instance, fixing γ-mercaptopropy-trimethoxysilane (γ-MPTMS) on the surface of γ-Al_2O_3 would improve its selectivity toward Cu, Hg, Au and Pd ions rather than other ions [32]. The XRD pattern shows that the modified γ-Al_2O_3 tends to be amorphous possibly because of the formation of chemical bond of Si–O–Al, which is more stable than physical loading. Three mechanisms were responsible for the adsorption of metal ions on γ-MPTMS modified nano-alumina: (1) metal ions adsorbed through the affinity of –SH, (2) the hydrolyzation of metal ions, and (3) electrostatic adsorption. In acidic media the first mechanism plays a dominant role while in basic solutions, the hydrolyzation and the electrostatic interactions play more significant role. Additionally, sodium dodecyl sulfate coated nano γ-Al_2O_3 (Fig. 3) was modified with 2,4-dinitrophenylhydrazine (DNPH) as a new solid-phase adsorbent for removal of trace Pb (II), Cr (III), Cd (II), Ni (II), Co (II) and Mn (II). SEM image showed that the naked alumina nanoparticles had a mean diameter of 53 nm, while that of the modified ones are in the range of 68–87 nm [101]. The BET surface area decreased from 42.62 m^2/g to 30.38 m^2/g after modification due to the bulk size of the organic ligand [102–105]. It was found that sorption isotherms were better described by Freundlich model for Mn (II), Pb (II), Cr (III) and Cd (II) ions and by Langmuir model for Ni (II) and Co (II) ions. The maximum adsorption capacity values of the modified alumina nanoparticles (q_m, calculated from Langmuir equation) toward Cr (III), Cd (II) and Pb (II) ions from multiple-metal solution (mixture of six metal ions) were 100.0, 83.33 and 100.0 mg/g, respectively [33].

2.4. Nanosized titanium oxides

It has been reported that bulk and nanoparticle TiO_2 anatase exhibit different chemical behavior, catalytic reactivity, and surface acidity based on their different surface planes [30,106,107]. Specific surface area of the nanosized and bulk particles were 185.5 and 9.5 m^2/g, and the nominal particle sizes calculated from BET measurements were 8.3 and 329.8 nm, respectively [30]. They had a $pH_{pzc} = 5.2$, which fell within the range of the results reported in the previous literatures [108,109]. The nanoparticles were able to simultaneously remove multiple metals (Zn, Cd, Pb, Ni, Cu) from a solution of pH = 8 and a San Antonio tap water. When adsorption capacities were normalized by mass, the nanoparticles adsorbed more than the bulk particles. However, as the results were surface-area normalized, the opposite tendency was observed. Adsorption kinetics for heavy metals followed a modified first order model, and the nanoparticles had a faster adsorption than the bulk ones. Langmuir isotherm was suitable to characterize metal adsorption onto TiO_2 anatase. By comparing the distribution coefficient (K_d), TiO_2 nanoparticles performed better than other metal oxide nanoparticles and a commercial activated carbon [30].

In another study conducted by Liang et al. [29], nano-TiO_2 (diameter = 10–50 nm, BET surface area = 208 m^2/g) showed adsorptive capacity to Zn and Cd as 15.3 and 7.9 mg/g, respectively, at pH = 9.0. The presence of common cations and anions (100–5000 mg/L) has no significant influence on the targeted metal (Zn^{2+} and Cd^{2+} ions of 1.0 mg/mL) adsorption under the given conditions.

2.5. Nanosized zinc oxides

As an environmental friendly material, ZnO can be used in catalyst industry [110,111], gas sensors [112], solar cells [113] and so on. As an adsorbent, ZnO was mostly applied to eliminate

Table 3
Adsorption capacities of Cr (VI) on different nano-MgOs [134].

Nano-MgOs	Commercial available	Nanoflakes	Mesoporous microspheres composed of nanoflakes	Rhombohedra	Microspheres composed of rhombohedra
BET surface area (m^2/g)	38	135	118	35	46
Cr (VI) (mg/g)	10.2	15.2	19.8	12.9	13.9

H_2S. Recently, people have found that nanostructured ZnO could efficiently remove heavy metals [35]. Lee et al. [114] prepared nanometer size zinc oxide (ZnO) powder by "solution-combustion method (SCM)". Compared with two titanium dioxide powders, P25 and one prepared by a homogeneous precipitation process at low temperature, the zinc oxide nanopowder showed higher removal rate of Cu^{2+} ions from the solution.

The plate-like nanostructured ZnO with high specific surface area was fabricated by various methods, such as hydrothermal [115–118], solvothermal [119], chemical vapor deposition [120,121], electrochemical deposition [122–124], and microwave method [112]. Besides some properties similar to TiO_2, ZnO nanoplates has many unique advantages, such as simple and cheap to prepare, convenient to tailor morphologically [34]. The solvothermal-prepared ZnO nanoplates [35] are composed of two terminal non-polar planes with several microns in the planar dimensions and 10–15 nm in thickness. The nanoplates are porous with a pore diameter of 5–20 nm and a high specific surface area (147 m^2/g). These nanoplates have an adsorption capacity of >1600 mg/g for Cu (II) ions. The adsorption isotherm is subject to the Freundlich equation (K_F = 324.22 (mg/g/mg)$^{-n}$, n = 4.56), while the commercial ZnO nanopowders follow a Langmuir isotherm model.

In addition, the metal sorbed nano-ZnO can be employed to fabricate other environmental materials. Ma et al. [34] reported a novel strategy to prepare ZnO/PbS heterostructured functional nanocomposite based on Pb^{2+} sorbed ZnO. In brief, ZnO nanosheets prepared via a hydrothermal approach were used to adsorb Pb^{2+} and then hydrothermally treated in aqueous solution containing sulfur source. Due to the surface hydroxy groups, the resultant ZnO nanosheets exhibited a good capacity to Pb^{2+} as 6.7 mg/g. The Pb^{2+}-preloaded ZnO nanosheets were put into a Telfon-lined stainless steel autoclave containing sulfur source at 120 °C for 12 h, and the resultant ZnO/PbS nanocomposite exhibits potential use in photocatalytic fields, energy-conversion devices and light-emitting/detecting devices. This new strategy seems also suitable for fabricating new materials based on other metal-loaded NMOs.

2.6. Nanosized magnesium oxides

Numerous works have focused on the synthesis of nanosized magnesium oxides of various morphologies, such as nanorods [125,126], fishbone fractal nanostructures induced by Co [127], nanowires [128,129], nanobelts [130], nanotubes [131] and three-dimensional entities [132], and nanocubes [133]. Gao et al. [134] developed a facile method to fabricate MgO of different morphologies and investigated their influence on the adsorption capacity to pollutants. By changing the concentration of Mg^{2+} and HCO_3^-, monoclinic $Mg_5(CO_3)_4(OH)_2(H_2O)_4$ with nanoflakes and flowerlike microspheres composed of flakes and hexagonal $MgCO_3$ with layer-like rhombohedra and microspheres composed of rhombohedra were synthesized. After annealing at 650 °C, four kinds of nano-MgO of mesoporous structures were obtained. It is a good example for the tunable synthesis of morphological nanoparticles by adjusting the components and the crystal phases of the precursors. The highly supersaturation of the reactant species is believed to be the driving force for the hierarchical growth.

Table 3 lists the adsorption capacities of MgO to Cr (VI). The novel structure of the microspheres improved the adsorption capability of MgO. The flowerlike mesoporous MgO microspheres also exhibited excellent adsorption capabilities to Cd (II) and Pb (II) [134]. At a contact time of 120 min, the concentration of Cd (II) and Pb (II) decreased from 100 mg/L to 0.007 mg/L and 0.05 mg/L, respectively, which are much lower than the Pollutant Dischargeable Standard in China (Cd (II) <0.01 mg/L, Pb (II) < 0.1 mg/L) and a little higher than MCLs for drinking water established by the Environmental Protection Agency (EPA) of the United States (Cd (II) <0.005 mg/L, Pb (II) < 0.015 mg/L).

2.7. Nanosized cerium oxides

Among cerium oxides, ceria is a most common and useful rare earth metal oxide in industrial applications, including catalysts, UV blocking and shielding materials, polishing materials, fuel cells, gas sensors, adsorbents, and luminescence [135–137]. The adsorptive properties of ceria vary significantly with morphologies, sizes, shapes and surface areas. Nanoscale effect further induces new properties for nanometer-sized ceria, such as new catalytic activity [138], blue shift in absorption spectra [139], lattice expansion [140], phase transformation [141], and photovoltaic response [142].

Ceria nanoparticles were synthesized by oxidation of Ce^{3+} to Ce^{4+} under alkaline conditions using hexamethylenetetramine (HMT) [143]. In this process, CeO_2 nanocrystals in solution can be stabilized by HMT through formation of double electrical layer, which is expected to prevent agglomeration of nanoparticles. The CeO_2 nanoparticles have a mean size of 12 nm, zeta potential of 11.5 mV, and BET surface area of 65 m^2/g. During the adsorption of Cr (VI) on ceria nanoparticles, no Cr (VI) was detected in the solid phase and the total Cr obtained was Cr (III). In the liquid phase only chromium (VI) was obtained, suggesting an Ox–Red process on the surface of the nanoparticle. The reduced chromium remains at the oxygen vacancy on the ceria surface. The isotherm was well described by the Freundlich adsorption model [144] with a correlation coefficient of R^2 = 0.955, whereas the kinetics corresponds to a pseudo-second-order equation. However, according to the results of bioluminescent test, the toxicity of the treated solution is not significantly altered after this treatment [37].

Besides nanoparticles, ceria has been successfully fabricated in other forms, such as nanorods [145], nanowires [146], nanotubes [129], nanopolyhedrons [147], three-dimensional flower-like structures [148], and hollow structures [149]. Cao et al. [36] provided a template-free microwave-assisted hydrothermal method to prepare ceria hollow nanospheres. Compared with template-based methods, such as soft template methods using organic surfactants [150,151] or hard template methods using solid templates [152,153], the template-free process is more economically desirable and environmentally benign. The hollow interior space effectively enhances the spatial dispersion, which results in not only higher surface area but also facile mass transportation of molecules to the active sites. The ceria hollow nanospheres have a uniform size of 260 nm and are composed of CeO_2 nanocrystals sized about 14 nm. They have a high surface area of 72 m^2/g. These ceria hollow nanospheres showed an apparent adsorption for heavy metal ions, for example, 15.4 mg/g for Cr (VI) and 9.2 mg/g for Pb (II) [36], which are nearly 70 times higher than that of the commercial bulk ceria material. The experimental data fit well with Langmuir adsorption model.

Table 4
Adsorption capacities of NMOs for heavy metals.

NMOs	Adsorption capacities of heavy metals (mg/g)					
	Pb	Cu	Cr	Cd	Zn	Ni
Goethite		149.25 [22]				
Hematite		84.46 [22]				
HFO	20.27 [23]					
HAO	20.27 [23]					
HMO	324.32 [26]			143.31 [26]	57.21 [26]	
Maghemite		26.8 [25]	19.2 [24] 17.0 [25]			23.6 [25]
α-MnO_2		82.6 [27]				
TiO_2	81.3 [30]			7.9 [29] 15.2 [30]	15.3 [29]	67.4 [30]
Al_2O_3						176.1 [31]
Modified Al_2O_3	100 [33]	16.3 [32]	100 [33]	83.33 [33]		18.18 [33]
ZnO	6.7 [34]	1600 [35]				
CeO_2	9.2 [36]	15.4 [36] 121.95 [37]				

Since there are so many types of NMOs employed for heavy metal removal, comparison of their capacity is necessary. However, the experimental conditions in the related references varied greatly and thus, direct comparison of the reported data seems a little meaningless. For example, due to the different synthetic methods of a given NMO, it is difficult to keep constant its size and surface chemistry. In addition, the operating conditions, like the solution chemistry (pH, ionic strength and ion types), temperature, experimental form (batch or column runs) are quite different from each other. Here, we just made a simple comparison on some typical NMOs for metal removal (Table 4).

3. Composition of NMOs with porous supports

3.1. Host-supported NMOs

NMOs provide an effective and specific adsorption toward heavy metals. Nevertheless, they are usually present as fine or ultrafine particles, which often lead to problems such as activity loss due to agglomeration, difficult separation, and excessive pressure drops when applied in flow-through systems [154]. An effective approach to overcome these technical bottlenecks is to fabricate hybrid adsorbents by impregnating or coating NMOs particles into/onto porous supports of larger size [155–158]. The widely used supports include natural hosts such as bentonite [159,160], sand [161,162], and montmorillonite [23], metallic oxide materials such as Al_2O_3 membrane [163] and porous manganese oxide complex [164], and synthetic polymer hosts such as cross-linked ion-exchange resins [165–167]. Some host-supported NMOs for heavy metal removal are summarized in Table 5.

3.1.1. Natural supports

Bentonite is a kind of huge-deposited natural clay with basic structural unit of two tetrahedrally coordinated sheets of silicon ions surrounding a sandwiched octahedrally coordinated sheet of aluminum ions. The structure results in a net negative surface charge on the clay [189]. Also, bentonite has amphoteric pH-dependent surfaces, high exchange capacity and different modes of aggregation [183], which makes it a potential adsorbent for adsorption of heavy metals from aqueous solutions [159].

Eren [159] ever coated the raw bentonite (RB) with iron and magnesium oxide for adsorptive removal of Pb (II) from aqueous solution. Both iron oxide-coated bentonite (ICB) and magnesium oxide-coated bentonite (MCB) were prepared by precipitating the metal ions with sodium hydroxide on the surface of raw bentonite, followed by thermal treatment. BET surface areas follow an order as ICB > RB > MCB. The Langmuir monolayer adsorption capacities of RB, ICB and MCB toward Pb (II) from 0.1 M KNO_3 solution were estimated to be 16.70, 22.20 and 31.86 mg/g, respectively. Similar results for the adsorption of Cr (III), Pb (II) and Zn (II) were reported by other researchers [190,191]. All the bentonite samples showed a similar behavior of increased uptake of Pb (II) with gradually increasing pH because H^+ can compete for the exchange site with Pb (II). Increasing the ionic strength from 0.01 to 0.1 M led to a significant decrease in Pb (II) adsorption. Besides, the adsorption of Pb (II) by the metal oxide-coated samples was influenced by the presence of Cl^- because Pb–Cl and PbOH–Cl complexes become the dominant Pb (II) species [159]. Thus, the specifically adsorbed ligand enhances Pb (II) retention by the surface complexation of Pb (II). Eren et al. [160] also studied magnesium oxide-coated bentonite for the removal of copper ions from aqueous solution. The adsorption of Cu (II) ions depends upon the nature of the adsorbent surface as well as the Cu (II) species distribution solution, which are greatly affected by the pH of the system. The values of the adsorption coefficients indicate the favorable nature of Cu (II) adsorption on the MCB. The Langmuir monolayer adsorption capacity of MCB in 0.1 M KNO_3 solution was estimated to be 58.44 mg/g, whereas the adsorption capacity of RB was 42.41 mg/g, indicating that the treatment with magnesium oxide increased the number of adsorption sites to a large extent, which may be attributed to an increase in surface charge due to the formation of magnesium oxide on the bentonite surface.

3.1.2. Metallic oxide supports

Nanofiltration membrane techniques have been introduced to remove metal ions from water [192]. One of the nanofiltration membranes, the anodic alumina membranes (AAM) has tunable holes [193], where NMOs of different size can be arrayed to fabricate composite adsorbents. Fig. 4 depicts a schematic process for preparation of hydrated MgO-nanotubes arrays within the alumina membranes [163]. The results of XRD spectrum and EDS pattern confirmed that hydrated MgO embedded on the AAM was crystalline. SEM images suggested that aligned nanotubes with uniform size and shape were obtained, and the diameters of the tubes were consistent with the pore diameters of AAM. This new adsorptive material was used for removal of Ni (II) from water. The equilibrium sorption capacity achieves 147.2 mg (Ni^{2+})/g $(Mg(OH)_2$, due to the adhering OH^- on the wall of $Mg(OH)_2$ nanotubes. Also, nickel ions replace magnesium ions to form $Ni(OH)_2$ because the solubility of $Ni(OH)_2$ ($K_{sp}{}^{298K} = 2.0 \times 10^{-15}$) is much lower than that of $Mg(OH)_2$ ($K_{sp}{}^{298K} = 1.2 \times 10^{-11}$). In addition, $Mg(OH)_2$ nanotubes have a large amount of activity sites owing to their high surface areas, unique needle-like morphology and nanocrystalline/amorphous structures [194]. Thus, sorption of nickel to $Mg(OH)_2$ is greatly

Table 5
Host-supported NMOs for heavy metal removal from water.

NMOs	Host substrate	Target metals	Removal performance	Refs.
Iron oxide	Treated municipal sewage sludge	Cu (II), Cd (II), Ni (II), Pb (II)	The maximum adsorption capacity for Cu (II), Cd (II), Ni (II) and Pb (II) was 17.3, 14.7, 7.8 and 42.4 mg/g, respectively.	[168]
	Sand	Cu (II)	24% removed at pH = 9	[169]
	Ferruginous sand	Cu (II), Ni (II)	Cu^{2+}: 2.04 mg/g (pH = 5) Ni^{2+}: 1 mg/g (pH = 7)	[170]
	Sand	Ni (II)	Batch test. 2.73 mg Ni/g adsorbent	[171]
	Graphene Nanosheets	Cr (VI)	From 28,670 ppb to below 10 ppb after being filtered for 5 times	[172]
	Bentonite	Pb (II)	31.86 mg/g	[159]
Goethite	Sand (quartz)	Cu (II), Pb (II)	0.259 mg Cu/g sand, 1.211 mg Pb/g sand	[173]
	Clinoptilolite	Cu (II) Mn (II) Zn (II)	0.5 mmol/g (Cu), 0.09 mmol/g (Mn), 0.2 mmol/g (Zn)	[174]
	Sand	Cd (II) Pb (II)	Maximum adsorption capacity values: 704 μg Cd/g sand at pH = 6, 702 μg Pb/g sand at pH = 5.0.	[175]
	Sand (quartz)	Cd (II)	0.2 mg/g at pH = 8	[176]
Hydrated ferric oxide	Polyacrylamide	Pb (II) Hg (II) Cd (II)	211.4 mg/g for Pb (II), 155.0 mg/g for Hg (II), 147.2 mg/g for Cd (II)	[177]
	Polymeric cation exchanger	Pb (II) Cu (II) Cd (II)	From 1 ppm to <5 ppb within 7000 BV	[178]
Fe_3O_4	Cyclodextrin	Cu (II)	47.2 mg/g	[52]
Fe_2O_3	Sepiolite	Ni (II)	18.30 mg/g	[179]
Manganese oxide	Crushed brick	Pb (II)	0.030 mmol/g	[180]
	Sand	Cr (VI) Cd (II)	0.326 mmol/g for Cr (VI) and 0.111 mmol/g for Cd (II)	[162]
	Sand	Ni (II)	3.33 mg/g	[171]
	Sand	Pb (II)	0.029 mmol/g	[180]
	Sand	Mn (II)	1.069 mg/g	[181]
	Silica	Mn (II)	0.396 mg/g	[161]
	Calcined-starfish	Mn (II)	1.480 mg/g	[181]
	Zeolite	Cu (II) Pb (II)	0.116 mmol/g, 0.349 mmol/g	[182]
	Unye bentonite	Cu (II)	105.38 mg/g	[183]
	Diatomite	Pb (II) Cd (II)	99.00 mg/g (Pb), 27.86 mg/g (Cd)	[184]
	Reduced Graphene oxide	Hg (II)	100% removal	[185]
Hydrous manganese oxide	Polymeric cation exchanger D-001, 001 × 7; D-113	Pb (II), Cd (II) Zn (II)	K_d increased by 20–800 times as compared to host exchangers, sorption capacities increased by 50–300%	[186]
Magnesium oxide	Bentonite	Cu (II)	58.44 mg/g	[160]
$Mg(OH)_2$/MgO	Al_2O_3 membranes	Ni (II)	147.2 mg/g ($Mg(OH)_2$)	[163]
ZnO	Activated carbon	Pb (II)	100% removal	[187]
Nanometer calcium titanate	Aluminum oxide	Pb (II) Cd (II) Zn (II)	124 mg/g (Pb), 8.58 mg/g (Cd) and 13.86 mg/g (Zn)	[188]

enhanced. Furthermore, the saturated $Mg(OH)_2$-nanotubes/Al_2O_3 composite membranes after sorbing nickel ions were thermally treated to convert $Mg(OH)_2$–$Ni(OH)_2$ to MgO–NiO. The MgO–NiO-nanotubes/Al_2O_3 composite membranes can be reused to remove Ni^{2+} from water with still high effectiveness [163].

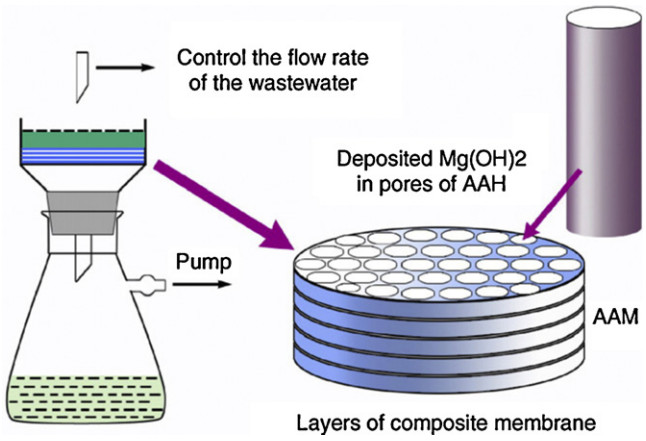

Fig. 4. Schematic illustration of fabrication of hydrated MgO-nanotubes/Al_2O_3 composite membranes and their nickel removal [163].

3.1.3. Manufactured polymer supports

Compared to other host materials, porous polymeric hosts are a particularly attractive option partly because of their controllable pore size and surface chemistry as well as their excellent mechanical strength for long-term use. A recent review is now available concerning polymer-based nanocomposite for environmental application by Zhao et al. [20]. The charged functional groups bound to the polymeric matrix are believed to enhance permeation of inorganic pollutants of counter charges, which can be interpreted by Donnan membrane principle [154,165,166,195,196]. A new hybrid adsorbent HMO-001, which was fabricated in our laboratory by impregnating nanosized hydrous manganese dioxide (HMO) onto a porous polystyrene cation exchanger resin (D-001), provided a nice example [166]. Basic structure and morphology of HMO-001 is depicted in Fig. 5. Lead adsorption onto HMO-001 was tested and the maximum capacity of HMO-001 toward lead ion was about 395 mg/g. As compared to a macroporous cation exchanger. D-001, HMO-001 exhibited highly selective lead retention from waters in the presence of competing Ca^{2+}, Mg^{2+}, and Na^{+} at high concentration levels. Fixed-bed column adsorption of a simulated water indicated that lead retention on HMO-001 resulted in a conspicuous decrease of this toxic metal from 1 mg/L to below 0.01 mg/L (the drinking water standard recommended by WHO). The exhausted adsorbent particles were amenable to regeneration by the binary NaAc–HAc solution for repeated use without noticeable capacity loss.

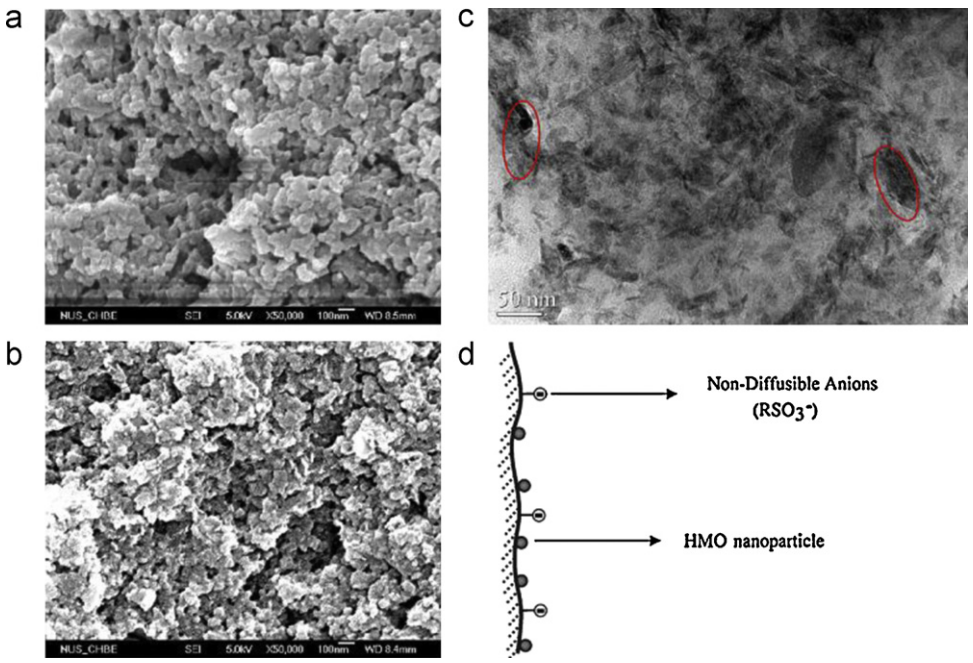

Fig. 5. (a) SEM of D-001, (b) SEM of HMO-001, (c) TEM of HMO-001, and (d) schematic illustration of HMO-001 [166].

3.2. Magnetic sorbents based On NMOs

Based on the magnetic characteristic of some NFeOs, composite sorbents with magnetism were fabricated for facile separation from the reaction systems. Some of them were synthesized by modifying the surface chemistry of the magnetic NFeOs with other materials of functional groups, including chitosan [75], *Sphaerotilus natans* [55], alginic acid [197], humic acid [53], amino [54], polyacrylic acid [19] and carboxymethyl-beta-cyclodextrin [52]. Others were obtained by encapsulating magnetic NFeOs with poly (3,4-ethylenedioxythiophene) [46], hydrogel [45] and SiO_2 [44]. Several porous materials such as zeolite [198], multiwall carbon nanotube [199], mesopore molecular sieve [200], graphene nanosheets [172] were also chosen as the substrates for supporting magnetic NFeOs. The available composite magnetic adsorbents exhibit satisfactory adsorption of toxic metals from aqueous solution.

3.2.1. Surface modification of magnetic NFeOs by amino group

Surface modification of the magnetic NFeOs is believed to prevent their aggregation [201,202] and air oxidation [69] in aqueous system. A novel magnetic nano-adsorbent has been developed by covalently binding polyacrylic acid (PAA) on the surface of Fe_3O_4 nanoparticles, followed by amino-functionalization using diethylenetriamine via carbodiimide activation [54] (Fig. 6). The amino-functionalized Fe_3O_4 nanoparticles were of 11.2 ± 2.8 nm in mean diameter and 63.2 emu/g in saturation magnetization. Adsorption of Cu (II) and Cr (VI) ions obeyed the Langmuir isotherm equation. The maximum adsorption capacities and Langmuir adsorption constants were 12.43 mg/g and 0.06 L/mg for Cu (II) ions and 11.24 mg/g and 0.0165 L/mg for Cr (VI) ions, respectively. Another PAA coated magnetic iron oxide nanoparticles (m-PAA-Na) were successfully prepared by coprecipitation, followed by modification with 3-aminopropyl triethoxysilane and acryloyl chloride [19]. The surface of the modified nanoparticles was further modified by graft polymerization with acrylic acid. With the size ranging from 10 to 23 nm, the magnetite nanoparticles exhibited superparamagnetism above 300 K, and the saturation magnetization was 57.1 emu/g at 300 K. m-PAA-Na could adsorb Cu^{2+}, Pb^{2+}, Ni^{2+} and Cd^{2+} well, and higher pH resulted in its higher chelation tendency. The amount of adsorption increased with the increase in temperature for all the metals.

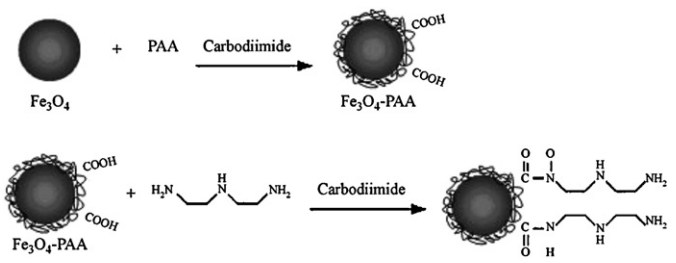

Fig. 6. A scheme for the binding and amino-fictionalization of PAA on Fe_3O_4 nanoparticles as a novel magnetic nano-adsorbent for both metal cation and anions [54].

3.2.2. Supporting magnetic NFeOs with zeolite

Zeolites offer an attractive and inexpensive option for the removal of organic and inorganic contaminants [203]. Natural zeolites are of low cost and can function as cation exchangers for metallic contaminants. The adsorption capacity of zeolite results from their high surface area and net negative charge on their channel structure, which attracts and holds cations such as heavy metals [204]. For example, NaY zeolites with pore diameter of 0.78 nm possess large surface area and high cation exchange capacity could serve as adsorbent for heavy metals [205–207].

Moreover, zeolite is also an excellent host for NFeOs encapsulation. Oliveira et al. [198] combined NaY zeolite with magnetic iron oxides to fabricate a magnetic adsorbent. The NaY zeolite:iron oxide magnetic composites were prepared at a weight ratio of 3:1, which was chosen to keep a relatively high content of iron oxide and thereafter to avoid the decrease in adsorption capacity of the composites. They were available by precipitation of iron oxides or hydroxides onto the zeolite surface. Fe oxide in the composites had a smaller particle size (ca. 25 nm for pure Fe oxide and ca. 16 nm for the composite). Due to the presence of 26% (w/w) of iron oxide, the composite showed decreased BET surface area (381 m^2/g) and micropore volume (0.148 cm^3/g) compared with the pure NaY

Table 6
Regeneration of heavy metals-preloaded NMOs.

Sorbents	Adsorbates	Regeneration/desorption		Refs.
		Reagent	Efficiency	
Maghemite	Cr (VI)	0.01 M NaOH	87.7%	[24]
Maghemite	Cu (II), Ni (II)	0.05 M HCl	Cu (II) 94.1% Ni (II) 93.4%	[25]
HMO	Pb (II), Cd (II), Zn (II)	0.5 M HCl	Pb (II) 89% Cd (II) 97% Zn (II) 99%	[26]
Al_2O_3	Co (II), Ni (II)	Chelate sorbents and diluted hydrochloric acid	–	[31]
Modified Al_2O_3	Hg (II), Cu (II), Au (II), Pd (II)	Diluted hydrochloric acid (pH > 3)	–	[32]
Modified Al_2O_3	Pb (II), Cd (II), Cr (II), Co (II), Ni (II), Mn (II)	1 mol L^{-1} HNO_3 + 1.5 mL of methanol	>97%	[33]
CeO_2	Pb (II), Cr (II)	0.1 M NaOH	64–75%	[36,37]

zeolite (568 m^2/g and 0.267 cm^3/g). The immobilized NFeOs are mainly present as maghemite along with some goethite. Upon controlled H_2 treatment the iron oxides can be reduced to metallic iron and the composite magnetization increased. The adsorption of Cu^{2+}, Cr^{3+} and Zn^{2+} from aqueous solutions on the 3:1 zeolite:Fe oxide composite was studied, and the adsorption capacity were in the order of $Cr^{3+} > Cu^{2+} > Zn^{2+}$.

3.2.3. Coating magnetic NFeOs with PEDOT

Poly(3,4-ethylenedioxythiophene) (PEDOT) contains sulfur endowing two unpaired electrons. The thiol-functionalized polymer is readily conjugated with positively charged heavy metal ions according to the coordination formation. Therefore, PEDOT functionalized magnetic nanoparticles are regarded as an excellent candidate for efficiently separable and reusable absorbent for heavy metal removal by using an external magnetic field [208–210].

Shin and Jang [46] provided a facile synthetic route for the fabrication of magnetic nanoparticle – PEDOT core–shell nanostructures. As illustrated in Fig. 7, it was achieved by inducing ferric cations onto the magnetic nanoparticles (MNPs) with a partial etching process followed by seeded polymerization. The amount of Ag^+, Hg^{2+} and Pb^{2+} uptake were ca. 27.96, 16.02 and 14.99 mmol/g, respectively. The adsorption rate was observed in the order of $Ag^+ > Hg^{2+} > Pb^{2+}$, in accordance with cation radius and interaction enthalpy values [211,212].

In addition, regeneration of metal-loaded NMOs is also an important feature to evaluate their repeatability in use and the possibility of recovering valuable metals from the eluates. In principle, the regeneration efficiency mainly depends upon the nature of metal adsorption, i.e., how metals interact with NMOs, as well as the components of the eluting reagents. Currently, studies on how to regenerate metal-loaded NMOs are limited as compared to the adsorption studies. This is partly because most of the available works focus on the performance of NMOs toward metal removal as well as the underlying mechanism. Comparatively, how to regenerate the used NMOs for multiple uses is ignored. Here we just summarized the results of some regeneration tests in Table 6. Obviously, more attention should be paid to the topic when we hope to promote environmental nanotechnology approaching to the practical application.

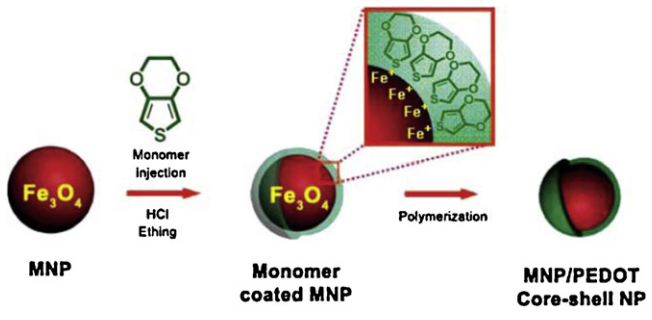

Fig. 7. The fabrication procedure of Fe_3O_4–PEDOT NPs by seeded polymerization mediated with acidic etching [46].

4. Conclusion and prospects

To date, NMOs are widely explored as highly efficient adsorbents for heavy metal removal from water/wastewater. They exhibit various advantages such as fast kinetics, high capacity, and preferable sorption toward heavy metals in water and wastewater. Nevertheless, to further promote the practical application of NMOs in abatement of heavy metal pollution, there still exist some technical bottlenecks to be solved. For instance, when applied in aqueous solution, NMOs tend to aggregate into large-size particles and their capacity loss seems inevitable. In addition, how to efficiently and costly separate the exhausted NMOs from water/wastewater still remains an interesting but challenging task. As for column operation, the excessive pressure drop caused by NMOs should also be considered. Fortunately, fabrication of new NMOs-based composite adsorbents seems to be an effective approach to respond to all the above technical problems. However, it is still in the infant stage, and various issues need to be solved concerning the development of more facile processes to obtain the composite adsorbents, the answer to the interplay between the hosts and the supported NMOs, the long-term performance of the composite adsorbents, as well as their field application in heavy metal contaminated water treatment.

Acknowledgements

The study was supported by NSFC (51078179/21177059), Jiangsu NSF (BK2009253) and the Ministry of Education of China (200802840034).

References

[1] M. Jamil, M.S. Zia, M. Qasim, Contamination of agro-ecosystem and human health hazards from wastewater used for irrigation, J. Chem. Soc. Pak. 32 (2010) 370–378.
[2] S. Khan, Q. Cao, Y.M. Zheng, Y.Z. Huang, Y.G. Zhu, Health risks of heavy metals in contaminated soils and food crops irrigated with wastewater in Beijing, China, Environ. Pollut. 152 (2008) 686–692.
[3] A. Singh, R.K. Sharma, M. Agrawal, F.M. Marshall, Health risk assessment of heavy metals via dietary intake of foodstuffs from the wastewater irrigated site of a dry tropical area of India, Food Chem. Toxicol. 48 (2010) 611–619.
[4] S.H. Peng, W.X. Wang, X.D. Li, Y.F. Yen, Metal partitioning in river sediments measured by sequential extraction and biomimetic approaches, Chemosphere 57 (2004) 839–851.
[5] F.L. Fu, Q. Wang, Removal of heavy metal ions from wastewaters: a review, J. Environ. Manage. 92 (2011) 407–418.
[6] Y.H. Wang, S.H. Lin, R.S. Juang, Removal of heavy metal ions from aqueous solutions using various low-cost adsorbents, J. Hazard. Mater. 102 (2003) 291–302.
[7] D.W. O'Connell, C. Birkinshaw, T.F. O'Dwyer, Heavy metal adsorbents prepared from the modification of cellulose: a review, Bioresour. Technol. 99 (2008) 6709–6724.
[8] T.A. Kurniawan, G.Y.S. Chan, W.H. Lo, S. Babel, Physico-chemical treatment techniques for wastewater laden with heavy metals, Chem. Eng. J. 118 (2006) 83–98.

[9] N. Galil, M. Rebhun, Primary chemical treatment minimizing dependence on bioprocess in small treatment plants, Water Sci. Technol. 22 (1990) 203–210.
[10] B.J. Pan, B.C. Pan, W.M. Zhang, L. Lv, Q.X. Zhang, S.R. Zheng, Development of polymeric and polymer-based hybrid adsorbents for pollutants removal from waters, Chem. Eng. J. 151 (2009) 19–29.
[11] S.P. Mishra, V.K. Singh, D. Tiwari, Radiotracer technique in adsorption study. 14. Efficient removal of mercury from aqueous solutions by hydrous zirconium oxide, Appl. Radiat. Isot. 47 (1996) 15–21.
[12] J.E. Vanbenschoten, B.E. Reed, M.R. Matsumoto, P.J. McGarvey, Metal removal by soil washing for an iron-oxide coated sandy soil, Water Environ. Res. 66 (1994) 168–174.
[13] J.A. Coston, C.C. Fuller, J.A. Davis, Pb^{2+} and Zn^{2+} adsorption by a natural aluminum-bearing and iron-bearing surface coating on an aquifer sand, Geochim. Cosmochim. Acta 59 (1995) 3535–3547.
[14] A. Agrawal, K.K. Sahu, Kinetic and isotherm studies of cadmium adsorption on manganese nodule residue, J. Hazard. Mater. 137 (2006) 915–924.
[15] A. Henglein, Small-particle research – physicochemical properties of extremely small colloidal metal and semiconductor particles, Chem. Rev. 89 (1989) 1861–1873.
[16] M.A. El-Sayed, Some interesting properties of metals confined in time and nanometer space of different shapes, Acc. Chem. Res. 34 (2001) 257–264.
[17] E.A. Deliyanni, E.N. Peleka, K.A. Matis, Modeling the sorption of metal ions from aqueous solution by iron-based adsorbents, J. Hazard. Mater. 172 (2009) 550–558.
[18] T. Pradeep, Anshup, Noble metal nanoparticles for water purification: a critical review, Thin Solid Films 517 (2009) 6441–6478.
[19] A.R. Mandavian, M.A.S. Mirrahimi, Efficient separation of heavy metal cations by anchoring polyacrylic acid on superparamagnetic magnetite nanoparticles through surface modification, Chem. Eng. J. 159 (2010) 264–271.
[20] X. Zhao, L. Lv, B. Pan, W. Zhang, S. Zhang, Q. Zhang, Polymer-supported nanocomposites for environmental application – a review, Chem. Eng. J. (2011).
[21] P.R. Grossl, D.L. Sparks, C.C. Ainsworth, Rapid kinetics of Cu(II) adsorption–desorption on goethite, Environ. Sci. Technol. 28 (1994) 1422–1429.
[22] Y.H. Chen, F.A. Li, Kinetic study on removal of copper (II) using goethite and hematite nano-photocatalysts, J. Colloid Interface Sci. 347 (2010) 277–281.
[23] M. Fan, T. Boonfueng, Y. Xu, L. Axe, T.A. Tyson, Modeling Pb sorption to microporous amorphous oxides as discrete particles and coatings, J. Colloid Interface Sci. 281 (2005) 39–48.
[24] J. Hu, G.H. Chen, I.M.C. Lo, Removal and recovery of Cr (VI) from wastewater by maghemite nanoparticles, Water Res. 39 (2005) 4528–4536.
[25] J. Hu, G.H. Chen, I.M.C. Lo, Selective removal of heavy metals from industrial wastewater using maghemite nanoparticle: Performance and mechanisms, J. Environ. Eng.-ASCE. 132 (2006) 709–715.
[26] Q. Su, B.C. Pan, S.L. Wan, W.M. Zhang, L. Lv, Use of hydrous manganese dioxide as a potential sorbent for selective removal of lead, cadmium, and zinc ions from water, J. Colloid Interface Sci. 349 (2010) 607–612.
[27] R. Koivula, J. Pakarinen, M. Sivenius, K. Sirola, R. Harjula, E. Paatero, Use of hydrometallurgical wastewater as a precursor for the synthesis of cryptomelane-type manganese dioxide ion exchange material, Sep. Purif. Technol. 70 (2009) 53–57.
[28] J. Pakarinen, R. Koivula, M. Laatikainen, K. Laatikainen, E. Paatero, R. Harjula, Nanoporous manganese oxides as environmental protective materials – effect of Ca and Mg on metals sorption, J. Hazard. Mater. 180 (2010) 234–240.
[29] P. Liang, T.Q. Shi, J. Li, Nanometer-size titanium dioxide separation/preconcentration and FAAS determination of trace Zn and Cd in water sample, Int. J. Environ. Anal. Chem. 84 (2004) 315–321.
[30] K.E. Engates, H.J. Shipley, Adsorption of Pb, Cd, Cu, Zn, and Ni to titanium dioxide nanoparticles: effect of particle size, solid concentration, and exhaustion, Environ. Sci. Pollut. Res. 18 (2011) 386–395.
[31] Y.I. Tarasevich, G.M. Klimova, Complex-forming adsorbents based on kaolinite, aluminium oxide and polyphosphates for the extraction and concentration of heavy metal ions from water solutions, Appl. Clay Sci. 19 (2001) 95–101.
[32] X.L. Pu, Z.C. Jiang, B. Hu, H.B. Wang, Gamma-MPTMS modified nanometer-sized alumina micro-column separation and preconcentration of trace amounts of Hg, Cu Au and Pd in biological, environmental and geological samples and their determination by inductively coupled plasma mass spectrometry, J. Anal. Atom. Spectrom. 19 (2004) 984–989.
[33] A. Afkhami, M. Saber-Tehrani, H. Bagheri, Simultaneous removal of heavy-metal ions in wastewater samples using nano-alumina modified with 2,4-dinitrophenylhydrazine, J. Hazard. Mater. 181 (2010) 836–844.
[34] X.F. Ma, Y.Q. Wang, M.J. Gao, H.Z. Xu, G.A. Li, A novel strategy to prepare ZnO/PbS heterostructured functional nanocomposite utilizing the surface adsorption property of ZnO nanosheets, Catal. Today 158 (2010) 459–463.
[35] X.B. Wang, W.P. Cai, Y.X. Lin, G.Z. Wang, C.H. Liang, Mass production of micro/nanostructured porous ZnO plates and their strong structurally enhanced and selective adsorption performance for environmental remediation, J. Mater. Chem. 20 (2010) 8582–8590.
[36] C.Y. Cao, Z.M. Cui, C.Q. Chen, W.G. Song, W. Cai, Ceria hollow nanospheres produced by a template-free microwave-assisted hydrothermal method for heavy metal ion removal and catalysis, J. Phys. Chem. C 114 (2010) 9865–9870.
[37] S. Recillas, J. Colon, E. Casals, E. Gonzalez, V. Puntes, A. Sanchez, X. Font, Chromium VI adsorption on cerium oxide nanoparticles and morphology changes during the process, J. Hazard. Mater. 184 (2010) 425–431.
[38] L. Li, M.H. Fan, R.C. Brown, J.H. Van Leeuwen, J.J. Wang, W.H. Wang, Y.H. Song, P.Y. Zhang, Synthesis, properties, and environmental applications of nanoscale iron-based materials: a review, Crit. Rev. Environ. Sci. Technol. 36 (2006) 405–431.
[39] A.L. Willis, N.J. Turro, S. O'Brien, Spectroscopic characterization of the surface of iron oxide nanocrystals, Chem. Mater. 17 (2005) 5970–5975.
[40] B.L. Cushing, V.L. Kolesnichenko, C.J. O'Connor, Recent advances in the liquid-phase syntheses of inorganic nanoparticles, Chem. Rev. 104 (2004) 3893–3946.
[41] J. Park, K.J. An, Y.S. Hwang, J.G. Park, H.J. Noh, J.Y. Kim, J.H. Park, N.M. Hwang, T. Hyeon, Ultra-large-scale syntheses of monodisperse nanocrystals, Nat. Mater. 3 (2004) 891–895.
[42] X. Wang, J. Zhuang, Q. Peng, Y.D. Li, A general strategy for nanocrystal synthesis, Nature 437 (2005) 121–124.
[43] Y. Ju-Nam, J.R. Lead, Manufactured nanoparticles: an overview of their chemistry, interactions and potential environmental implications, Sci. Total Environ. 400 (2008) 396–414.
[44] J. Wang, S. Zheng, Y. Shao, J. Liu, Z. Xu, D. Zhu, Amino-functionalized Fe_3O_4@SiO_2 core–shell magnetic nanomaterial as a novel adsorbent for aqueous heavy metals removal, J. Colloid Interface Sci. 349 (2010) 293–299.
[45] S.C.N. Tang, P. Wang, K. Yin, I.M.C. Lo, Synthesis and application of magnetic hydrogel for Cr (VI) removal from contaminated water, Environ. Eng. Sci. 27 (2010) 947–954.
[46] S. Shin, J. Jang, Thiol containing polymer encapsulated magnetic nanoparticles as reusable and efficiently separable adsorbent for heavy metal ions, Chem. Commun. (2007) 4230–4232.
[47] G. Pan, Y.W. Qin, X.L. Li, T.D. Hu, Z.Y. Wu, Y.N. Xie, EXAFS studies on adsorption–desorption reversibility at manganese oxides–water interfaces. I. Irreversible adsorption of zinc onto manganite (gamma-MnOOH), J. Colloid Interface Sci. 271 (2004) 28–34.
[48] X.L. Li, G. Pan, Y.W. Qin, T.D. Hu, Z.Y. Wu, Y.N. Xie, EXAFS studies on adsorption–desorption reversibility at manganese oxide–water interfaces. II. Reversible adsorption of zinc on delta-MnO_2, J. Colloid Interface Sci. 271 (2004) 35–40.
[49] S. Shironita, M. Goto, T. Kamegawa, K. Mori, H. Yamashita, Preparation of highly active platinum nanoparticles on ZSM-5 zeolite including cerium and titanium dioxides as photo-assisted deposition sites, Catal. Today 153 (2010) 189–192.
[50] J.E. Macdonald, J.G.C. Veinot, Removal of residual metal catalysts with iron/iron oxide nanoparticles from coordinating environments, Langmuir 24 (2008) 7169–7177.
[51] E.A. Deliyanni, N.K. Lazaridis, E.N. Peleka, K.A. Matis, Metals removal from aqueous solution by iron-based bonding agents, Environ. Sci. Pollut. Res. 11 (2004) 18–21.
[52] A.Z.M. Badruddoza, A.S.H. Tay, P.Y. Tan, K. Hidajat, M.S. Uddin, Carboxymethyl-beta-cyclodextrin conjugated magnetic nanoparticles as nano-adsorbents for removal of copper ions: Synthesis and adsorption studies, J. Hazard. Mater. 185 (2011) 1177–1186.
[53] J.F. Liu, Z.S. Zhao, G.B. Jiang, Coating Fe_3O_4 magnetic nanoparticles with humic acid for high efficient removal of heavy metals in water, Environ. Sci. Technol. 42 (2008) 6949–6954.
[54] S.H. Huang, D.H. Chen, Rapid removal of heavy metal cations and anions from aqueous solutions by an amino-functionalized magnetic nano-adsorbent, J. Hazard. Mater. 163 (2009) 174–179.
[55] X.-h. Guan, Y.-c. Qin, L.-w. Wang, R. Yin, M. Lu, Y.-j. Yang, Study on the disposal process for removing heavy metal ions from wastewater by composite biosorbent of nano Fe_3O_4/*Sphaerotilus natans*, Chin. J. Environ. Sci. 28 (2007) 436–440.
[56] U. Schwertmann, R.M. Taylor, Natural and synthetic poorly crystallized lepidocrocite, Clay Miner. 14 (1979) 285–293.
[57] K. Hachiya, M. Sasaki, T. Ikeda, N. Mikami, T. Yasunaga, Static and kinetic-studies of adsorption desorption of metal-ions on a gamma-Al_2O_3 surface. 2. kinetic-study by means of pressure-jump technique, J. Phys. Chem. 88 (1984) 27–31.
[58] K.F. Hayes, J.O. Leckie, Pressure-jump kinetic-studies of lead-ion adsorption at the goethite aqueous interface, Abstr. Am. Chem. Soc. 193 (1987) 205–209.
[59] M. Eigen, K. Tamm, Schallabsorption in elektrolytlosungen als folge chemischer relaxation. 2. messergebnisse und relaxationsmechanismen fur 2-2-wertige elektrolyte, Z. Elektrochem. 66 (1962) 107–121.
[60] D.A. Dzombak, F.M.M. Morel, Sorption of cadmium on hydrous ferric-oxide at high sorbate/sorbent ratios – equilibrium, kinetics, and modeling, J. Colloid Interface Sci. 112 (1986) 588–598.
[61] K.C. Swallow, D.N. Hume, F.M.M. Morel, Sorption of copper and lead by hydrous ferric-oxide, Environ. Sci. Technol. 14 (1980) 1326–1331.
[62] P. Trivedi, J.A. Dyer, D.L. Sparks, Lead sorption onto ferrihydrite. 1. A macroscopic and spectroscopic assessment, Environ. Sci. Technol. 37 (2003) 908–914.
[63] T.N.D. Dantas, A.A.D. Neto, M. Moura, Removal of chromium from aqueous solutions by diatomite treated with microemulsion, Water Res. 35 (2001) 2219–2224.
[64] C.H. Weng, J.H. Wang, C.P. Huang, Adsorption of Cr (VI) onto TiO_2 from dilute aqueous solutions, Water Sci. Technol. 35 (1997) 55–62.
[65] S. Babel, T.A. Kurniawan, Cr (VI) removal from synthetic wastewater using coconut shell charcoal and commercial activated carbon modified with oxidizing agents and/or chitosan, Chemosphere 54 (2004) 951–967.

[66] F.N. Acar, E. Malkoc, The removal of chromium (VI) from aqueous solutions by *Fagus orientalis* L., Bioresour. Technol. 94 (2004) 13–15.
[67] P. Tartaj, M.D. Morales, S. Veintemillas-Verdaguer, T. Gonzalez-Carreno, C.J. Serna, The preparation of magnetic nanoparticles for applications in biomedicine, J. Phys. D: Appl. Phys. 36 (2003) 182–197.
[68] P. Tartaj, M.P. Morales, T. Gonzalez-Carreno, S. Veintemillas-Verdaguer, C.J. Serna, Advances in magnetic nanoparticles for biotechnology applications, J. Magn. Magn. Mater. 290 (2005) 28–34.
[69] D. Maity, D.C. Agrawal, Synthesis of iron oxide nanoparticles under oxidizing environment and their stabilization in aqueous and non-aqueous media, J. Magn. Magn. Mater. 308 (2007) 46–55.
[70] S.E. Khalafalla, G.W. Reimers, Preparation of dilution-stable aqueous magnetic fluids, IEEE Trans. Magn. 16 (1980) 178–183.
[71] L. Fu, V.P. Dravid, D.L. Johnson, Self-assembled (SA) bilayer molecular coating on magnetic nanoparticles, Appl. Surf. Sci. 181 (2001) 173–178.
[72] J. Dobson, T.G.S. Pierre, H. Pardoe, P. Schultheiss-Grassi, Experimental and theoretical evaluation of the interaction of biogenic magnetite with magnetic fields, in: S. Bersani (Ed.), Electricity and Magnetism in Biology and Medicine, Plenum, New York, 1999, pp. 401–404.
[73] R.S. Molday, D. Mackenzie, Immunospecific ferromagnetic iron-dextran reagents for the labeling and magnetic separation of cells, J. Immunol. Methods 52 (1982) 353–367.
[74] A. Pathak, A.B. Panda, A. Tarafdar, P. Pramanik, Synthesis of nano-sized metal oxide powders and their application in separation technology, J. Indian Chem. Soc. 80 (2003) 289–296.
[75] Y.C. Chang, D.H. Chen, Preparation and adsorption properties of monodisperse chitosan-bound Fe_3O_4 magnetic nanoparticles for removal of Cu(II) ions, J. Colloid Interface Sci. 283 (2005) 446–451.
[76] A.F. Ngomsik, A. Bee, M. Draye, G. Cote, V. Cabuil, Magnetic nano- and microparticles for metal removal and environmental applications: a review, C.R. Chim. 8 (2005) 963–970.
[77] Y.S. Kang, S. Risbud, J.F. Rabolt, P. Stroeve, Synthesis and characterization of nanometer-size Fe3O4 and γ-Fe2O3 particles, Chem. Mater. (1996) 2209–2211.
[78] C.L. Warner, R.S. Addleman, A.D. Cinson, T.C. Droubay, M.H. Engelhard, M.A. Nash, W. Yantasee, M.G. Warner, High-performance, superparamagnetic, nanoparticle-based heavy metal sorbents for removal of contaminants from natural waters, ChemSusChem 3 (2010) 749–757.
[79] H.Q. Wang, G.F. Yang, Q.Y. Li, X.X. Zhong, F.P. Wang, Z.S. Li, Y.H. Li, Porous nano-MnO_2: large scale synthesis via a facile quick-redox procedure and application in a supercapacitor, New J. Chem. 35 (2011) 469–475.
[80] P. Larger-Trivedi, L. Axe, A comparison of strontium sorption to hydrous aluminum, iron, and manganese oxides, J. Colloid Interface Sci. 218 (1999) 554–563.
[81] S.P. Mishra, Vijaya, Removal behavior of hydrous manganese oxide and hydrous stannic oxide for Cs (I) ions from aqueous solutions, Sep. Purif. Technol. 54 (2007) 10–17.
[82] S.P. Mishra, S.S. Dubey, D. Tiwari, Rapid and efficient removal of Hg (II) by hydrous manganese and tin oxides, J. Colloid Interface Sci. 279 (2004) 61–67.
[83] T. Takamatsu, M. Kawashima, M. Koyama, The role of Mn^{2+}-rich hydrous manganese oxide in the accumulation of arsenic in lake-sediments, Water Res. 19 (1985) 1029–1032.
[84] M. Kawashima, Y. Tainaka, T. Hori, M. Koyama, T. Takamatsu, Phosphate adsorption onto hydrous manganese (IV) oxide in the presence of divalent-cations, Water Res. 20 (1986) 471–475.
[85] S.S. Tripathy, J.L. Bersillon, K. Gopal, Adsorption of Cd^{2+} on hydrous manganese dioxide from aqueous solutions, Desalination 194 (2006) 11–21.
[86] M.I. Zaman, S. Mustafa, S. Khan, B.S. Xing, Effect of phosphate complexation on Cd^{2+} sorption by manganese dioxide (beta-MnO_2), J. Colloid Interface Sci. 330 (2009) 9–19.
[87] K.M. Parida, S.B. Kanungo, B.R. Sant, Studies on MnO_2. 1. chemical-composition, microstructure and other characteristics of some synthetic MnO_2 of various crystalline modifications, Electrochim. Acta 26 (1981) 435–443.
[88] R.R. Gadde, H.A. Laitinen, Studies of heavy-metal sorption by hydrous oxides, Abstr. Am. Chem. Soc. (1974) 142.
[89] M. Misono, E.I. Ochiai, Y. Saito, Y. Yoneda, A new dual parameter scale for strength of lewis acids and bases with evaluation of their softness, J. Inorg. Nucl. Chem. 29 (1967) 2685–2691.
[90] R.N. Deguzman, Y.F. Shen, E.J. Neth, S.L. Suib, C.L. Oyoung, S. Levine, J.M. Newsam, Synthesis and characterization of octahedral molecular-sieves (OMS-2) having the hollandite structure, Chem. Mater. 6 (1994) 815–821.
[91] X.H. Feng, F. Liu, W.F. Tan, X.W. Liu, Synthesis of birnessite from the oxidation of Mn^{2+} by O^{2-} in alkali medium: effects of synthesis conditions, Clays Clay Miner. 52 (2004) 240–250.
[92] A. Dyer, M. Pillinger, J. Newton, R. Harjula, T. Moller, S. Amin, Sorption behavior of radionuclides on crystalline synthetic tunnel manganese oxides, Chem. Mater. 12 (2000) 3798–3804.
[93] M. Tsuji, S. Komarneni, Selective exchange of divalent transition-metal ions in cryptomelane-type manganic acid with tunnel structure, J. Mater. Res. 8 (1993) 611–616.
[94] J.D. Li, Y.L. Shi, Y.Q. Cai, S.F. Mou, G.B. Jiang, Adsorption of di-ethyl-phthalate from aqueous solutions with surfactant-coated nano/microsized alumina, Chem. Eng. J. 140 (2008) 214–220.
[95] M. Hiraide, J. Iwasawa, S. Hiramatsu, H. Kawaguchi, Use of surfactant aggregates formed on alumina for the preparation of chelating sorbents, Anal. Sci. 11 (1995) 611–615.
[96] G. Chang, Z. Jiang, T. Peng, B. Hu, Preparation of high-specific-surface-area nanometer-sized alumina by sol–gel method and study on adsorption behaviors of transition metal ions on the alumina powder with ICP-AES, Acta Chim. Sinica 61 (2003).
[97] M. Hiraide, M.H. Sorouradin, H. Kawaguchi, Immobilization of dithizone on surfactant-coated alumina for preconcentration of metal-ions, Anal. Sci. 10 (1994) 125–127.
[98] M. Ghaedi, K. Niknam, A. Shokrollahi, E. Niknam, H.R. Rajabi, M. Soylak, Flame atomic absorption spectrometric determination of trace amounts of heavy metal ions after solid phase extraction using modified sodium dodecyl sulfate coated on alumina, J. Hazard. Mater. 155 (2008) 121–127.
[99] S. Dadfarnia, A.M.H. Shabani, H.D. Shirie, Determination of lead in different samples by atomic absorption spectrometry after preconcentration with dithizone immobilized on surfactant-coated alumina, Bull. Korean Chem. Soc. 23 (2002) 545–548.
[100] A.M.H. Shabani, S. Dadfarnia, Z. Dehghani, On-line solid phase extraction system using 1,10-phenanthroline immobilized on surfactant coated alumina for the flame atomic absorption spectrometric determination of copper and cadmium, Talanta 79 (2009) 1066–1070.
[101] D.J. Yang, B. Paul, W.J. Xu, Y. Yuan, E.M. Liu, X.B. Ke, R.M. Wellard, C. Guo, Y. Xu, Y.H. Sun, H.Y. Zhu, Alumina nanofibers grafted with functional groups: a new design in efficient sorbents for removal of toxic contaminants from water, Water Res. 44 (2010) 741–750.
[102] S. Brunauer, P.H. Emmett, E. Teller, Adsorption of gases in multimolecular layers, J. Am. Chem. Soc. 60 (1938) 309–319.
[103] R. Celis, M.C. Hermosin, J. Cornejo, Heavy metal adsorption by functionalized clays, Environ. Sci. Technol. 34 (2000) 4593–4599.
[104] Y. Mao, B.M. Fung, Formation and characterization of anchored polymer coatings on alumina, Chem. Mater. 10 (1998) 509–517.
[105] K.S. Walton, R.Q. Snurr, Applicability of the BET method for determining surface areas of microporous metal-organic frameworks, J. Am. Chem. Soc. 129 (2007) 8552–8556.
[106] G. Martra, Lewis acid and base sites at the surface of microcrystalline TiO_2 anatase: relationships between surface morphology and chemical behaviour, Appl. Catal. A: Gen. 200 (2000) 275–285.
[107] D.E. Giammar, C.J. Maus, L.Y. Xie, Effects of particle size and crystalline phase on lead adsorption to titanium dioxide nanoparticles, Environ. Eng. Sci. 24 (2007) 85–95.
[108] K.A.D. Guzman, M.P. Finnegan, J.F. Banfield, Influence of surface potential on aggregation and transport of titania nanoparticles, Environ. Sci. Technol. 40 (2006) 7688–7693.
[109] M. Kosmulski, The significance of the difference in the point of zero charge between rutile and anatase, Adv. Colloid Interface Sci. 99 (2002) 255–264.
[110] H.B. Zeng, W.P. Cai, P.S. Liu, X.X. Xu, H.J. Zhou, C. Klingshirn, H. Kalt, ZnO-based hollow nanoparticles by selective etching: Elimination and reconstruction of metal–semiconductor interface, improvement of blue emission and photocatalysis, ACS Nano 2 (2008) 1661–1670.
[111] G.H Chen, B.S. Fu, C.J. Cai, M.Q. Lu, Y. Yang, S.H. Yi, C. Xu, H. Li, G.S. Wang, T. Zhang, A single-center experience of retransplantation for liver transplant recipients with a failing graft, Transplant. Proc. 40 (2008) 1485–1487.
[112] Z.H. Jing, J.H. Zhan, Fabrication, Gas-sensing properties of porous ZnO nanoplates, Adv. Mater. 20 (2008) 4547–4551.
[113] T.P. Chou, Q.F. Zhang, G.E. Fryxell, G.Z. Cao, Hierarchically structured ZnO film for dye-sensitized solar cells with enhanced energy conversion efficiency, Adv. Mater. 19 (2007) 2588–2592.
[114] J.H. Lee, B.S. Kim, J.C. Lee, S. Park, Removal of Cu++ ions from aqueous Cu-EDTA solution using ZnO nanopowder, in: H.S. Kim, S.-Y. Park, B.Y. Hur, S.W. Lee (Eds.), Eco-Materials Processing & Design Vi, Trans Tech Publications, Korea, 2005, pp. 510–513.
[115] T.M. Shang, J.H. Sun, Q.F. Zhou, M.Y. Guan, Controlled synthesis of various morphologies of nanostructured zinc oxide: flower, nanoplate, and urchin, Cryst. Res. Technol. 42 (2007) 1002–1006.
[116] F. Xu, Z.Y. Yuan, G.H. Du, T.Z. Ren, C. Bouvy, M. Halasa, B.L. Su, Simple approach to highly oriented ZnO nanowire arrays: large-scale growth, photoluminescence and photocatalytic properties, Nanotechnology 17 (2006) 588–594.
[117] X.L Cao, H.B. Zeng, M. Wang, X.J. Xu, M. Fang, S.L. Ji, L.D. Zhang, Large scale fabrication of quasi-aligned ZnO stacking nanoplates, J. Phys. Chem. C 112 (2008) 5267–5270.
[118] P. Liu, G.W. She, Z.L. Liao, Y. Wang, Z.Z. Wang, W.S. Shi, X.H. Zhang, S.T. Lee, D.M. Chen, Observation of persistent photoconductance in single ZnO nanotube, Appl. Phys. Lett. 94 (2009).
[119] T. Ghoshal, S. Kar, S. Chaudhuri, ZnO doughnuts: controlled synthesis, growth mechanism, and optical properties, Cryst. Growth Des. 7 (2007) 136–141.
[120] N. Zhang, R. Yi, R.R. Shi, G.H. Gao, G. Chen, X.H. Liu, Novel rose-like ZnO nanoflowers synthesized by chemical vapor deposition, Mater. Lett. 63 (2009) 496–499.
[121] C. Xu, D. Kim, J. Chun, K. Rho, B. Chon, S. Hong, T. Joo, Temperature-controlled growth of ZnO nanowires and nanoplates in the temperature range 250–300 degrees C, J. Phys. Chem. B 110 (2006) 21741–21746.
[122] B.Q. Cao, X.M. Teng, S.H. Heo, Y. Li, S.O. Cho, G.H. Li, W.P. Cai, Different ZnO nanostructures fabricated by a seed-layer assisted electrochemical route and their photoluminescence and field emission properties, J. Phys. Chem. C 111 (2007) 2470–2476.

[123] B.Q. Cao, W.P. Cai, H.B. Zeng, G.T. Duan, Morphology evolution and photoluminescence properties of ZnO films electrochemically deposited on conductive glass substrates, Jpn. J. Appl. Phys. 99 (2006).
[124] B. Illy, B.A. Shollock, J.L. MacManus-Driscoll, M.P. Ryan, Electrochemical growth of ZnO nanoplates, Nanotechnology 16 (2005) 320–324.
[125] A.M. Cao, J.S. Hu, H.P. Liang, L.J. Wan, Self-assembled vanadium pentoxide (V_2O_5) hollow microspheres from nanorods and their application in lithium-ion batteries, Angew. Chem. Int. Ed. 44 (2005) 4391–4395.
[126] M. Mo, J.C. Yu, L.Z. Zhang, S.K.A. Li, Self-assembly of ZnO nanorods and nanosheets into hollow microhemispheres and microspheres, Adv. Mater. 17 (2005) 756–760.
[127] Y.Q. Zhu, W.K. Hsu, W.Z. Zhou, M. Terrones, H.W. Kroto, D.R.M. Walton, Selective Co-catalysed growth of novel MgO fishbone fractal nanostructures, Chem. Phys. Lett. 347 (2001) 337–343.
[128] Y.D. Yin, G.T. Zhang, Y.N. Xia, Synthesis and characterization of MgO nanowires through a vapor-phase precursor method, Adv. Funct. Mater. 12 (2002) 293–298.
[129] C.C. Tang, Y. Bando, T. Sato, Oxide-assisted catalytic growth of MgO nanowires with uniform diameter distribution, J. Phys. Chem. B 106 (2002) 7449–7452.
[130] Y.B. Li, Y. Bando, T. Sato, Preparation of network-like MgO nanobelts on Si substrate, Chem. Phys. Lett. 359 (2002) 141–145.
[131] J.H. Zhan, Y. Bando, J.P. Hu, D. Golberg, Bulk synthesis of single-crystalline magnesium oxide nanotubes, Inorg. Chem. 43 (2004) 2462–2464.
[132] K.L. Klug, V.P. Dravid, Observation of two- and three-dimensional magnesium oxide nanostructures formed by thermal treatment of magnesium diboride powder, Appl. Phys. Lett. 81 (2002) 1687–1689.
[133] S. Stankic, M. Muller, O. Diwald, M. Sterrer, E. Knozinger, J. Bernardi, Size-dependent optical properties of MgO nanocubes, Angew. Chem. Int. Ed. 44 (2005) 4917–4920.
[134] C.L. Gao, W.L. Zhang, H.B. Li, L.M. Lang, Z. Xu, Controllable fabrication of mesoporous MgO with various morphologies and their absorption performance for toxic pollutants in water, Cryst. Growth Des. 8 (2008) 3785–3790.
[135] S. Yabe, T. Sato, Cerium oxide for sunscreen cosmetics, J. Solid State Chem. 171 (2003) 7–11.
[136] L.Y. Wang, K.L. Zhang, Z.T. Song, S.L. Feng, Ceria concentration effect on chemical mechanical polishing of optical glass, Appl. Surf. Sci. 253 (2007) 4951–4954.
[137] E.L. Brosha, R. Mukundan, D.R. Brown, F.H. Garzon, J.H. Visser, Development of ceramic mixed potential sensors for automotive applications, Solid State Ionics 148 (2002) 61–69.
[138] S. Carrettin, P. Concepcion, A. Corma, J.M.L. Nieto, V.F. Puntes, Nanocrystalline CeO_2 increases the activity of an for CO oxidation by two orders of magnitude, Angew. Chem. Int. Ed. 43 (2004) 2538–2540.
[139] S. Tsunekawa, T. Fukuda, A. Kasuya, Blue shift in ultraviolet absorption spectra of monodisperse CeO_{2-x} nanoparticles, Jpn. J. Appl. Phys. 87 (2000) 1318–1321.
[140] S. Tsunekawa, K. Ishikawa, Z.Q. Li, Y. Kawazoe, A. Kasuya, Origin of anomalous lattice expansion in oxide nanoparticles, Phys. Rev. Lett. 85 (2000) 3440–3443.
[141] Z.W. Wang, S.K. Saxena, V. Pischedda, H.P. Liermann, C.S. Zha, In situ X-ray diffraction study of the pressure-induced phase transformation in nanocrystalline CeO_2, Phys. Rev. B: Condens. Matter 64 (2001).
[142] A. Corma, P. Atienzar, H. Garcia, J.Y. Chane-Ching, Hierarchically mesostructured doped CeO_2 with potential for solar-cell use, Nat. Mater. 3 (2004) 394–397.
[143] F. Zhang, Q. Jin, S.W. Chan, Ceria nanoparticles: size, size distribution, and shape, Jpn. J. Appl. Phys. 95 (2004) 4319–4326.
[144] S. Bernal, J.J. Calvino, M.A. Cauqui, J.M. Gatica, C. Larese, J.A.P. Omil, J.M. Pintado, Some recent results on metal/support interaction effects in NM/CeO_2 (NM: noble metal) catalysts, Catal. Today 50 (1999) 175–206.
[145] X.W. Liu, K.B. Zhou, L. Wang, B.Y. Wang, Y.D. Li, Oxygen vacancy clusters promoting reducibility and activity of ceria nanorods, J. Am. Chem. Soc 131 (2009) 3140–3141.
[146] T.Y. Yu, J. Joo, Y.I. Park, T. Hyeon, Large-scale nonhydrolytic sol–gel synthesis of uniform-sized ceria nanocrystals with spherical, wire, and tadpole shapes, Angew. Chem. Int. Ed. 44 (2005) 7411–7414.
[147] R. Si, Y.W. Zhang, L.P. You, C.H. Yan, Rare-earth oxide nanopolyhedra, nanoplates, and nanodisks, Angew. Chem. Int. Ed. 44 (2005) 3256–3260.
[148] L.S. Zhong, J.S. Hu, A.M. Cao, Q. Liu, W.G. Song, L.J. Wan, 3D flowerlike ceria micro/nanocomposite structure and its application for water treatment and CO removal, Chem. Mater. 19 (2007) 1648–1655.
[149] N.C. Strandwitz, G.D. Stucky, Hollow microporous cerium oxide spheres templated by colloidal silica, Chem. Mater. 21 (2009) 4577–4582.
[150] C.T. Kresge, M.E. Leonowicz, W.J. Roth, J.C. Vartuli, J.S. Beck, Ordered mesoporous molecular-sieves synthesized by a liquid-crystal template mechanism, Nature 359 (1992) 710–712.
[151] P.D. Yang, D.Y. Zhao, D.I. Margolese, B.F. Chmelka, G.D. Stucky, Generalized syntheses of large-pore mesoporous metal oxides with semicrystalline frameworks, Nature 396 (1998) 152–155.
[152] S.W. Bian, Z. Ma, W.G. Song, Preparation, Characterization of carbon nitride nanotubes and their applications as catalyst supporter, J. Phys. Chem. C 113 (2009) 8668–8672.
[153] S.W. Bian, Z. Ma, L.S. Zhang, F. Niu, W.G. Song, Silica nanotubes with mesoporous walls and various internal morphologies using hard/soft dual templates, Chem. Commun. (2009) 1261–1263.
[154] L. Cumbal, A.K. Sengupta, Arsenic removal using polymer-supported hydrated iron (III) oxide nanoparticles: role of Donnan membrane effect, Environ. Sci. Technol. 39 (2005) 6508–6515.
[155] M. Jang, W.F. Chen, F.S. Cannon, Preloading hydrous ferric oxide into granular activated carbon for arsenic removal, Environ. Sci. Technol. 42 (2008) 3369–3374.
[156] K.L. Chen, S.E. Mylon, M. Elimelech, Enhanced aggregation of alginate-coated iron oxide (hematite) nanoparticles in the presence of calcium, strontium, and barium cations, Langmuir 23 (2007) 5920–5928.
[157] B.O Hansen, P. Kwan, M.M. Benjamin, C.W. Li, G.V. Korshin, Use of iron oxide-coated sand to remove strontium from simulated hanford tank wastes, Environ. Sci. Technol. 35 (2001) 4905–4909.
[158] J.M. Zachara, S.C. Smith, L.S. Kuzel, Adsorption and dissociation of co-EDTA complexes in iron oxide-containing subsurface sands, Geochim. Cosmochim. Acta 59 (1995) 4825–4844.
[159] E. Eren, Removal of lead ions by Unye (Turkey) bentonite in iron and magnesium oxide-coated forms, J. Hazard. Mater. 165 (2009) 63–70.
[160] E. Eren, A. Tabak, B. Eren, Performance of magnesium oxide-coated bentonite in removal process of copper ions from aqueous solution, Desalination 257 (2010) 163–169.
[161] P.Y. Hu, Y.H. Hsieh, J.C. Chen, C.Y. Chang, Characteristics of manganese-coated sand using SEM and EDAX analysis, J. Colloid Interface Sci. 272 (2004) 308–313.
[162] S.M. Lee, W.G. Kim, C. Laldawngliana, D. Tiwari, Removal behavior of surface modified sand for Cd(II) and Cr(VI) from aqueous solutions, J. Chem. Eng. Data 55 (2010) 3089–3094.
[163] S. Zhang, F.Y. Cheng, Z.L. Tao, F. Gao, J. Chen, Removal of nickel ions from wastewater by Mg(OH)(2)/MgO nanostructures embedded in Al_2O_3 membranes, J. Alloys Compd. 426 (2006) 281–285.
[164] J. Otsu, Y. Oshima, New approaches to the preparation of metal or metal oxide particles on the surface of porous materials using supercritical water: development of supercritical water impregnation method, J. Supercrit. Fluids 33 (2005) 61–67.
[165] B.J. Pan, H. Qiu, B.C. Pan, G.Z. Nie, L.L. Xiao, L. Lv, W.M. Zhang, Q.X. Zhang, S.R. Zheng, Highly efficient removal of heavy metals by polymer-supported nanosized hydrated Fe (III) oxides: behavior and XPS study, Water Res. 44 (2010) 815–824.
[166] Q. Su, B.C. Pan, B.J. Pan, Q.R. Zhang, W.M. Zhang, L. Lv, X.S. Wang, J. Wu, Q.X. Zhang, Fabrication of polymer-supported nanosized hydrous manganese dioxide (HMO) for enhanced lead removal from waters, Sci. Total Environ. 407 (2009) 5471–5477.
[167] S.L. Wan, X. Zhao, L. Lv, Q. Su, H.N. Gu, B.C. Pan, W.M. Zhang, Z.W. Lin, J.F. Luan, Selective adsorption of Cd (II) and Zn (II) ions by nano-hydrous manganese dioxide (HMO)-encapsulated cation exchanger, Ind. Eng. Chem. Res. 49 (2010) 7574–7579.
[168] S. Babel, T.A. Kurniawan, Low-cost adsorbents for heavy metals uptake from contaminated water: a review, J. Hazard. Mater. 97 (2003) 219–243.
[169] P. Bose, M.A. Bose, S. Kumar, Critical evaluation of treatment strategies involving adsorption and chelation for wastewater containing copper, zinc and cyanide, Adv. Environ. Res. 7 (2002) 179–195.
[170] N. Boujelben, J. Bouzid, Z. Elouear, Adsorption of nickel and copper onto natural iron oxide-coated sand from aqueous solutions: study in single and binary systems, J. Hazard. Mater. 163 (2009) 376–382.
[171] N. Boujelben, J. Bouzid, Z. Elouear, M. Feki, Retention of nickel from aqueous solutions using iron oxide and manganese oxide coated sand: kinetic and thermodynamic studies, Environ. Technol. 31 (2010) 1623–1634.
[172] H.Y. Koo, H.J. Lee, H.A. Go, Y.B. Lee, T.S. Bae, J.K. Kim, W.S. Choi, Graphene-based multifunctional iron oxide nanosheets with tunable properties, Chem. Eur. J. 17 (2011) 1214–1219.
[173] C.H. Lai, C.Y. Chen, Removal of metal ions and humic acid from water by iron-coated filter media, Chemosphere 44 (2001) 1177–1184.
[174] M.K. Doula, Simultaneous removal of Cu, Mn and Zn from drinking water with the use of clinoptilolite and its Fe-modified form, Water Res. 43 (2009) 3659–3672.
[175] C.H. Lai, C.Y. Chen, B.L. Wei, C.W. Lee, Adsorptive characteristics of cadmium and lead on the goethite-coated sand surface, J. Environ. Sci. Health A 36 (2001) 747–763.
[176] C.H. Lai, C.Y. Chen, B.L. Wei, S.H. Yeh, Cadmium adsorption on goethite-coated sand in the presence of humic acid, Water Res. 36 (2002) 4943–4950.
[177] G.N. Manju, K.A. Krishnan, V.P. Vinod, T.S. Anirudhan, An investigation into the sorption of heavy metals from wastewaters by polyacrylamide-grafted iron (III) oxide, J. Hazard. Mater. 91 (2002) 221–238.
[178] B.C. Pan, B.J. Pan, W.M. Zhang, Q.J. Zhang, Q.R. Zhang, P.J. Jiang, Q.X. Zhang, Chinese patent: CN 200710191355.3 (2007).
[179] S. Lazarevic, I. Jankovic-Castvan, V. Djokic, Z. Radovanovic, D. Janackovic, R. Petrovic, Iron-modified sepiolite for Ni^{2+} sorption from aqueous solution: an equilibrium, kinetic, and thermodynamic study, J. Chem. Eng. Data 55 (2010) 5681–5689.
[180] N. Boujelben, J. Bouzid, Z. Elouear, Removal of lead (II) ions from aqueous solutions using manganese oxide-coated adsorbents: characterization and kinetic study, Adsorpt. Sci. Technol. 27 (2009) 177–191.
[181] S.M. Lee, W.G. Kim, J.K. Yang, D. Tiwari, Sorption behaviour of manganese-coated calcined-starfish and manganese-coated sand for Mn (II), Environ. Technol. 31 (2010) 445–453.

[182] R.P. Han, W.H. Zou, H.K. Li, Y.H. Li, J. Shi, Copper (II) and lead (II) removal from aqueous solution in fixed-bed columns by manganese oxide coated zeolite, J. Hazard. Mater. 137 (2006) 934–942.
[183] E. Eren, Removal of copper ions by modified Unye clay, Turkey, J. Hazard. Mater. 159 (2008) 235–244.
[184] M.A.M. Khraisheh, Y.S. Al-Degs, W.A.M. McMinn, Remediation of wastewater containing heavy metals using raw and modified diatomite, Chem. Eng. J. 99 (2004) 177–184.
[185] T.S. Sreeprasad, S.M. Maliyekkal, K.P. Lisha, T. Pradeep, Reduced graphene oxide–metal/metal oxide composites: facile synthesis and application in water purification, J. Hazard. Mater. 186 (2011) 921–931.
[186] B.C. Pan, Q. Su, W.M. Zhang, Q.X. Zhang, H.Q. Ren, Q.R. Zhang, B.J. Pan, Chinese patent: CN 101224408A (2008).
[187] Y. Kikuchi, Q.R. Qian, M. Machida, H. Tatsumoto, Effect of ZnO loading to activated carbon on Pb (II) adsorption from aqueous solution, Carbon 44 (2006) 195–202.
[188] D. Zhang, Preparation, Characterization of nanometer calcium titanate immobilized on aluminum oxide and its adsorption capacity for heavy metal ions in water, Adv. Mater. Res. 152–153 (2010) 670–673.
[189] P.F. Luckham, S. Rossi, The colloidal and rheological properties of bentonite suspensions, Adv. Colloid Interface Sci. 82 (1999) 43–92.
[190] A. Sari, M. Tuzen, M. Soylak, Adsorption of Pb (II) and Cr (III) from aqueous solution on Celtek clay, J. Hazard. Mater. 144 (2007) 41–46.
[191] K.G. Bhattacharyya, S. Sen Gupta, Adsorption of Fe (III) from water by natural and acid activated clays: Studies on equilibrium isotherm, kinetics and thermodynamics of interactions, Adsorption 12 (2006) 185–204.
[192] P. Cote, D. Mourato, C. Gungerich, J. Russell, E. Houghton, Immersed membrane filtration for the production of drinking water: case studies, Desalination 117 (1998) 181–188.
[193] M. Lahav, T. Sehayek, A. Vaskevich, I. Rubinstein, Nanoparticle nanotubes, Angew. Chem. Int. Ed. 42 (2003) 5575–5579.
[194] S. Utamapanya, K.J. Klabunde, J.R. Schlup, Nanoscale metal-oxide particles clusters as chemical reagents – synthesis and properties of ultrahigh surface-area magnesium-hydroxide and magnesium-oxide, Chem. Mater. 3 (1991) 175–181.
[195] B.J. Pan, J. Wu, B.C. Pan, L. Lv, W.M. Zhang, L.L. Xiao, X.S. Wang, X.C. Tao, S.R. Zheng, Development of polymer-based nanosized hydrated ferric oxides (HFOs) for enhanced phosphate removal from waste effluents, Water Res. 43 (2009) 4421–4429.
[196] Q.R. Zhang, P.J. Jiang, B.C. Pan, W.M. Zhang, L. Lv, Impregnating zirconium phosphate onto porous polymers for lead removal from waters: effect of nanosized particles and polymer chemistry, Ind. Eng. Chem. Res. 48 (2009) 4495–4499.
[197] C. Jeon, I.W. Nah, K.Y. Hwang, Adsorption of heavy metals using magnetically modified alginic acid, Hydrometallurgy 86 (2007) 140–146.
[198] L.C.A. Oliveira, D.I. Petkowicz, A. Smaniotto, S.B.C. Pergher, Magnetic zeolites: a new adsorbent for removal of metallic contaminants from water, Water Res. 38 (2004) 3699–3704.
[199] C.L. Chen, J. Hu, D.D. Shao, J.X. Li, X.K. Wang, Adsorption behavior of multiwall carbon nanotube/iron oxide magnetic composites for Ni (II) and Sr (II), J. Hazard. Mater. 164 (2009) 923–928.
[200] X.Q. Chen, K.F. Lam, Q.J. Zhang, B.C. Pan, M. Arruebo, K.L. Yeung, Synthesis of highly selective magnetic mesoporous adsorbent, J. Phys. Chem. C 113 (2009) 9804–9813.
[201] E. Illes, E. Tombacz, The role of variable surface charge and surface complexation in the adsorption of humic acid on magnetite, Colloids Surf. A 230 (2003) 99–109.
[202] E. Illes, E. Tombacz, The effect of humic acid adsorption on pH-dependent surface charging and aggregation of magnetite nanoparticles, J. Colloid Interface Sci. 295 (2006) 115–123.
[203] H.H. Murray, Traditional new applications for kaolin, smectite, and palygorskite: a general overview, Appl. Clay Sci. 17 (2000) 207–221.
[204] F. Cadena, R. Rizvi, R.W. Peter, Feasibility studies for the removal of heavy metal from solution using tailored bentonite, hazardous and industrial wastes, in: Proceedings 22nd Mid Atlantic Industrial Waste Conference, Drexel University, 1990, p. 77.
[205] K. Ryachi, A. Bencheikh, Characterization of some materials applied to depollution of waste liquid, Ann. Chim. Sci. Mater. 23 (1998) 393–396.
[206] Y.P. de Pena, W. Lopez, J.L. Burguera, M. Burguera, M. Gallignani, R. Brunetto, P. Carrero, C. Rondon, F. Imbert, Synthetic zeolites as sorbent material for on-line preconcentration of copper traces and its determination using flame atomic absorption spectrometry, Anal. Chim. Acta 403 (2000) 249–258.
[207] M. Trgo, J. Peric, Interaction of the zeolitic tuff with Zn-containing simulated pollutant solutions, J. Colloid Interface Sci. 260 (2003) 166–175.
[208] T.W. Kang, J. Moon, S. Oh, S.R. Hong, S. Chah, J.H. Yi, Direct observation of a cooperative mechanism in the adsorption of heavy metal ions to thiolated surface by in-situ surface plasmon resonance measurements, Chem. Commun. (2005) 2360–2362.
[209] L.M. Rossi, F.P. Silva, L.L.R. Vono, P.K. Kiyohara, E.L. Duarte, R. Itri, R. Landers, G. Machado, Superparamagnetic nanoparticle-supported palladium: a highly stable magnetically recoverable and reusable catalyst for hydrogenation reactions, Green Chem. 9 (2007) 379–385.
[210] A.M. Liu, K. Hidajat, S. Kawi, D.Y. Zhao, A new class of hybrid mesoporous materials with functionalized organic monolayers for selective adsorption of heavy metal ions, Chem. Commun. (2000) 1145–1146.
[211] Y. Takahashi, H. Kasai, H. Nakanishi, T.M. Suzuki, Test strips for heavy-metal ions fabricated from nanosized dye compounds, Angew. Chem. Int. Ed. 45 (2006) 913–916.
[212] J. Hu, I.M.C. Lo, G.H. Chen, Fast removal and recovery of Cr (VI) using surface-modified jacobsite ($MnFe_2O_4$) nanoparticles, Langmuir 21 (2005) 11173–11179.